Mechanical stochastic tug-of-war models cannot explain bidirectional lipid-droplet transport

Ambarish Kunwar[a,1], Suvranta K. Tripathy[b,1], Jing Xu[b,c], Michelle K. Mattson[b], Preetha Anand[b], Roby Sigua[b], Michael Vershinin[d], Richard J. McKenney[e], Clare C. Yu[f], Alexander Mogilner[a,2,3], and Steven P. Gross[b,2,3]

[a]Department of Neurobiology, Physiology and Behavior, University of California, Davis, CA 95616; [b]Department of Developmental and Cell Biology, University of California, Irvine, CA 92697; [f]Department of Physics and Astronomy, University of California, Irvine, CA 92697; [d]Department of Physics and Astronomy, University of Utah, Salt Lake City, UT 84112; and [e]Department of Pathology and Cell Biology, Columbia University, New York, NY 10032 [c]School of Natural Sciences, University of California, Merced, CA 95343

Edited by Charles S. Peskin, New York University, New York, NY, and approved September 15, 2011 (received for review May 18, 2011)

Intracellular transport via the microtubule motors kinesin and dynein plays an important role in maintaining cell structure and function. Often, multiple kinesin or dynein motors move the same cargo. Their collective function depends critically on the single motors' detachment kinetics under load, which we experimentally measure here. This experimental constraint—combined with other experimentally determined parameters—is then incorporated into theoretical stochastic and mean-field models. Comparison of modeling results and in vitro data shows good agreement for the stochastic, but not mean-field, model. Many cargos in vivo move bidirectionally, frequently reversing course. Because both kinesin and dynein are present on the cargos, one popular hypothesis explaining the frequent reversals is that the opposite-polarity motors engage in unregulated stochastic tugs-of-war. Then, the cargos' motion can be explained entirely by the outcome of these opposite-motor competitions. Here, we use fully calibrated stochastic and mean-field models to test the tug-of-war hypothesis. Neither model agrees well with our in vivo data, suggesting that, in addition to inevitable tugs-of-war between opposite motors, there is an additional level of regulation not included in the models.

Bidirectional motion of subcellular cargos such as mRNA particles, virus particles, endosomes, and lipid droplets is quite common (1), driven by plus-end kinesin and minus-end dynein. Bidirectional motion emerges when frequent switches occur between travel directions, and travel direction reflects which motor (s) dominates. Cells can regulate the switching frequency to control "net" transport, but the physical mechanism(s) underlying this control remains open. Two mechanisms have been proposed. The first suggests that plus-end and minus-end motors always engage in stochastic unregulated tugs-of-war, and overall cargo motion is explained by the outcomes of these mechanical tugs-of-war. This model was proposed theoretically to explain lipid-droplet motion (2) but has been adopted to explain endosome motion (3, 4). An alternative model suggests that in addition to competition between opposite-polarity motors, there is a "switch" mechanism or mechanisms that achieve further coordination between the motors. Such regulation may be dynamic (5), static (6), or a combination of the two. The crucial question is this: Can tug-of-war models, which exclusively consider cargos with fixed distributions of motors moving along microtubules unaffected by regulatory pathways, explain the characteristics of motility in vivo? Alternatively, are there significant motility characteristics not captured by tug-of-war models, pointing to a richer transport subsystem with important regulatory contributions?

There are two theoretical approaches to modeling collective motor transport. The mean-field approach (Fig. 1*A*) assumes all engaged motors share load equally (7). The stochastic model (Fig. 1*B*) simulates individual motors going through their mechanochemical cycle (8), where each motor's movement is determined by the load the cargo applies to that motor. The external load on the cargo and instantaneous positions of each motor define the cargo's position. Thus, different motors in the group move with different rates and experience different instantaneous forces; the cargo mechanically couples the motors. Each unidirectional model is the basis for a corresponding bidirectional tug-of-war model (Fig. 1 *C* and *D*).

Here, we consider both classes of models and compare theoretical predictions with experimentally observed motility. We start with models maximally constrained by experimental observations of single-motor behavior and then relax these constraints to investigate both quantitative and qualitative differences between model predictions and actual data. We note that motor detachment kinetics under high load affect motors' ensemble function (9), but complete data was not available. We thus measured single-motor detachment kinetics in the superstall regime and used this to constrain the models. The stochastic unidirectional model quantitatively captured multiple-motor function as measured experimentally in vitro, but the mean-field model did not. In vivo, neither model explains bidirectional lipid-droplet motion.

Results

Experimental Measurement of Kinesin and Dynein Detachment Kinetics. Kinesin's superforce off rate was reported as 2/s (10), and limited measurements showed that dynein's off rate slightly above stall was about 10/s (9). Here, we measured the off rates more systematically, using an optical trap–based method. We rapidly increased the force on a moving bead (*SI Text*) and measured the time to detachment (Fig. 2*A*, kinesin; Fig. 2*B*, dynein). From such events, we determined the detachment time distributions for specific superforce values, shown, e.g., for kinesin and dynein at approximately twice the stall force (Fig. 2 *C* and *D*) (see also *SI Text*). The detachment times for each superforce value are summarized for kinesin (Fig. 2*E*) and dynein (Fig. 2*F*). In contrast to a possible constant off rate (10), kinesin had an off rate increasing with force. At low loads, dynein is sensitive to load, detaching easily (9), but at higher load it exhibited a catch-bond type behavior, with off rate decreasing with load. The superforce experiments also allowed us to determine the probability of backward stepping for the motors. Kinesin (11) and dynein (12) can back-step under load, but this was relatively rare in both directions (<20%), and the typical backward travel distance was short, so we believe it is functionally irrelevant with regard to the behavior of kinesin or

Author contributions: A.K., S.K.T., C.C.Y., A.M., and S.P.G. designed research; A.K. and S.K.T. performed research; A.K., S.K.T., J.X., M.K.M., P.A., R.S., M.V., and R.J.M. contributed new reagents/analytic tools; A.K., S.K.T., A.M., and S.P.G. analyzed data; and A.K., S.K.T., A.M., and S.P.G. wrote the paper.

The authors declare no conflict of interest.

This article is a PNAS Direct Submission.

[1]A.K. and S.K.T. contributed equally to this work.

[2]A.M. and S.P.G. contributed equally to this work.

[3]To whom correspondence may be addressed. E-mail: mogilner@math.ucdavis.edu or sgross@uci.edu.

This article contains supporting information online at www.pnas.org/lookup/suppl/doi:10.1073/pnas.1107841108/-/DCSupplemental.

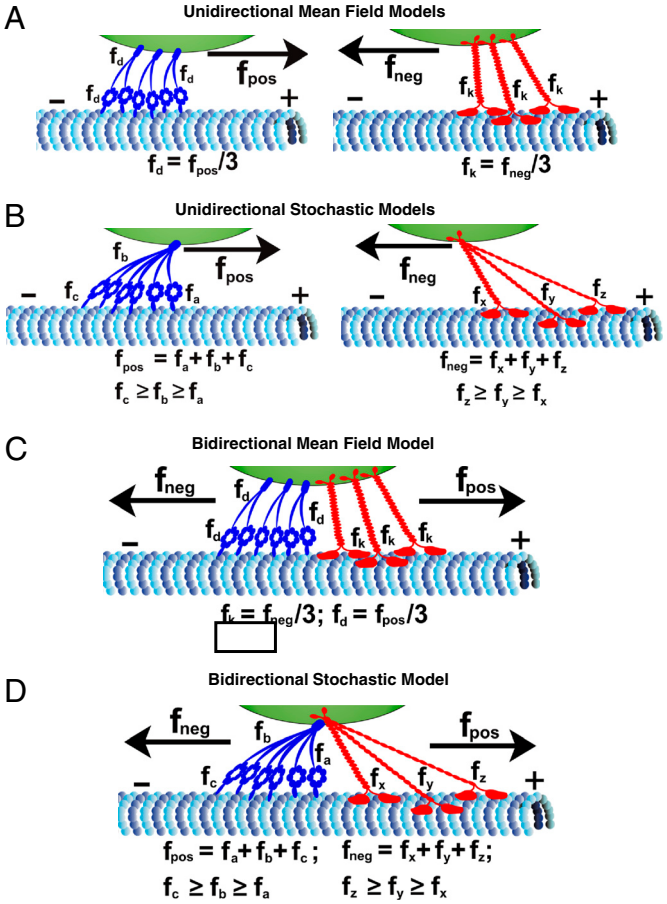

Fig. 1. Models of unidirectional (*A* and *B*) and bidirectional (*C* and *D*) transport schematic illustrations of a cargo (green) moved by $N = 3$ kinesin (red) or dynein (dark blue) motors, as modeled by the mean-field theory (*A*) or the stochastic model (*B*). Overall forces opposing motion (f_{pos},f_{neg}) are distributed equally in the mean-field model (f_d per dynein, f_k per kinesin), but not in the stochastic model (f_a–f_c for dynein, f_x–f_z for kinesin). (*C* and *D*) A tug-of-war between kinesin and dynein, as modeled in the mean-field theory (*C*) where motors share load equally, or the stochastic model (*D*) where they need not.

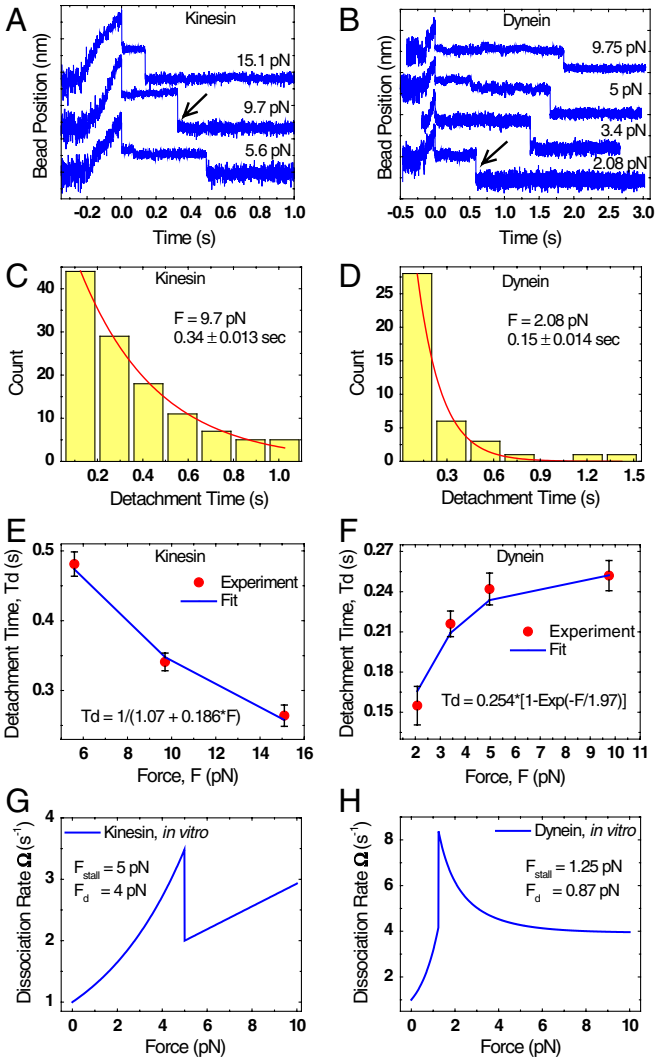

Fig. 2. Experimental characterization of in vitro single-molecule kinesin and dynein detachment kinetics. (*A* and *B*): Examples of experimental data traces. Beads with a single active kinesin (*A*) or dynein (*B*) (binding fraction < 0.35) were brought in contact with the microtubule at saturating ATP. Motion started (at approximately −0.2 s in these plots), causing displacement of the bead from the optical-trap center (traces start increasing). At a predefined displacement (here occurring at $t = 0$), the laser power was automatically increased, applying enough force to stall the moving bead (plateau immediately after $t = 0$). After a delay, the motor detached from the microtubule (black arrow), allowing the bead to rapidly return to the trap center. By controlling optical-trap power, we controlled the applied force. The detachment time was the interval between when trap power increased and when the bead detached; a histogram of such times is shown for one specific force for kinesin (*C*) and dynein (*D*). The characteristic detachment times were determined by fitting with decaying exponentials (red curves in *C* and *D*); the results of such fits are summarized in *E* and *F* for kinesin and dynein, respectively. *G* and *H* show the complete in vitro force-dissociation rate curves including detachment probabilities below stall (see *SI Text*).

dynein ensembles opposing each other. It was not included in our theoretical model.

Development of a Stochastic Unidirectional Theoretical Model for Kinesin and Dynein. Our older stochastic models for kinesin (8), and dynein (9, 13) were experimentally verified under some conditions (8, 9, 13). Here, we incorporate the measured detachment data into these models. The force-dissociation rate below stall is given by $\Omega(F) = \exp(F/Fd)$, as determined previously to match experimental data (8, 9). In the superstall regime, it was obtained by using simple fitting functions to approximate the measured detachment rates in Fig. 2 *E* and *F*. For kinesin, it was $\Omega(F) = 1.07 + 0.186 * F$, and for dynein was $\Omega(F) = 1/(0.254 * [1 - \exp(-F/1.97))$. The stall forces for kinesin and dynein were 4.7 ± 0.04 pN and 1.36 ± 0.02 pN, respectively, determined from in vitro stall-force distributions (see the *Definitions of the Stall Force (F_s) and Detachment Force (F_d) and Their Measurements* section in *SI Text*). F_d was the average detachment force obtained from experimental data (4.01 ± 0.07 pN for kinesin and 0.87 ± 0.04 pN for dynein). The dissociation rate near stall may be smoother than assumed in our model, but the model correctly captures the decline of the dissociation rate above stall. Associated corrections, if any, are not expected to alter the conclusions of this paper. The complete force-dissociation relations in our model are summarized in Fig. 2 *G* and *H* (see also *SI Text*).

Comparison of Stochastic and Mean-Field Theories with in Vitro Experiments for Unidirectional Motion: Detachment Times for Two-Motor Superstall Experiments. We experimentally tested the newly constrained theories using detachment times under superstall for two-motor events. With moderate motor density, beads are mostly moved by single motors, but are occasionally moved by two (motor density is chosen to make three-motor events rare). If a bead in a parabolic potential produced by an optical trap moved past a well-defined threshold force (slightly larger than F_s for a single motor), it was moved by two motors, and software increased the laser power abruptly to put the two motors into the

superstall regime. We then measured the detachment time distribution, for either kinesin (Fig. 3*A*) or dynein (Fig. 3*B*).

Constrained experimentally by measured single-molecule properties, and setting the total number of motors N equal to 2 instead of 1, there is only a single "free" parameter for the models, the single-motor on rate. Others have measured this to be approximately 5/s for kinesin (at saturating microtubule concentration), so we used this value; for dynein, it was a fitting parameter, and 5/s yielded the best description of the data. From the experimental distributions we calculated the mean detachment time, and then compared this with the predicted mean detachment times for the stochastic and mean-field theories (Fig. 3 *A* and *B*). The stochastic theory's predictions were consistent with experiments, but the mean-field predictions were not (Fig. 3 *C* and *D*), either when we assumed real experimental detachment kinetics, or when we assumed nonexperimental exponential detachment kinetics as has been done previously (7). Relative to the mean-field model, motors in the stochastic model were less sensitive to detachment under load (see *SI Text*).

The in Vivo Case: Model for a Bidirectional Tug-of-War. Given the stochastic model's in vitro success, we used it to develop a bidirectional tug-of-war model. We used the in vitro–measured detachment kinetics above stall, and other experimental constraints. First, our previous in vivo measurements established that in the absence of specific mutations, the forces powering plus-end and minus-end lipid-droplet motion were approximately the same (14), so any theoretical model must conform to this. Second, although the mechanism is currently unknown, our in vivo data suggests that the unitary (single-motor) stall force in each direction is approximately 2.5 pN, which is different from its value in vitro, so we decreased the kinesin stall force, and increased the dynein stall force (resulting in scaled force-dissociation curves shown in *SI Text*). Third, our recent quantitative measurements of droplet motion in phase II of *Drosophila* development (14) indicated that typically a few, but up to a maximum of four to five, motors could be instantaneously active. We assumed that in vivo on rates are the same as in vitro (i.e., approximately 5/s for both kinesin, and dynein) and that the motors had the same stiffness in vivo as in vitro. To constrain processivity, we purified kinesin from *Drosophila* embryos, and measured its single-molecule processivity to be 1.3 μm (*SI Text*). We have not yet determined *Drosophila* dynein's processivity, but assume it to be the same as for bovine dynein in the presence of dynactin (approximately 2.0 μm). With these constraints, we developed a stochastic tug-of-war model, as indicated in Fig. 1*D*. We estimate that the effective cytosolic viscosity affecting droplet motion is approximately 10× that of water, so that value was used in the simulations.

Thus, we implemented a bidirectional stochastic model with $N = 5$ motors. After incorporating the above experimental constraints, there were no free parameters; the model yielded simulated traces such as those shown in Fig. 4*B*. Using our parsing program (15), these traces were processed in the same way as for real motion, and a variety of metrics were compared to experimental values (see next).

Comparing in Vivo Experimental Data to the Stochastic Bidirectional Model. Our past studies developed multiple metrics to charac-

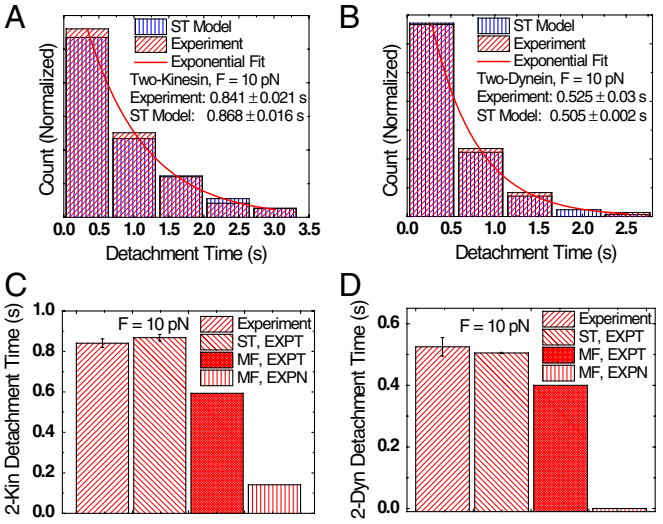

Fig. 3. Comparison of experimental measurements and theoretical predictions for detachment kinetics of two kinesin or dynein motors. Experiments were done as in Fig. 2 *A* and *B*, but a higher concentration of motors was used, so there was a small probability of having two simultaneously engaged motors. These relatively rare events were detected by force measurements: When a bead was moved further from the trap center than possible for a single motor (experimentally a threshold of 5.2 and 2.0 pN was used, for kinesin or dynein, respectively), the laser power was automatically increased to provide a superstall force. The distribution of detachment times (experimental bars, red hash marks; *A* and *B*) was compared to theory (parameter values in *SI Text*). The single-molecule properties (including single-motor detachment kinetics as measured in Fig. 2) constrained the model parameters. Using these constraints, the stochastic model (ST) with experimental detachment kinetics (EXPT) correctly predicted both the shape of the detachment distribution (*A* and *B*) and the correct average detachment time for both kinesin and dynein (*C* and *D*, respectively). The mean-field model with the same detachment kinetics did not, and the mean-field model with exponential detachment kinetics (EXPN) was even worse.

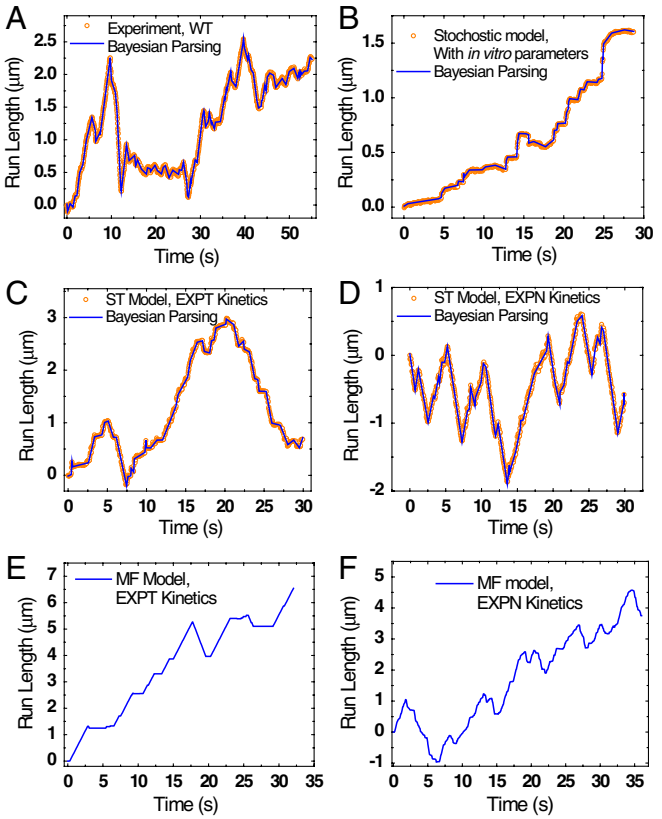

Fig. 4. Examples of experimental (*A*) and simulated (*B–F*) trajectories of single bidirectionally moving lipid droplets, projected along the axis of microtubules. For experimental data (*A*) and stochastically simulated motion (*B–D*), the properties of motion (run lengths and velocities, pause durations, etc.) were determined by parsing the motion identically using a Bayesian approach (15). The blue line corresponds to run and pause segments as parsed. For the mean-field model variants (*E* and *F*), the segments were determined directly.

terize motion. Individual lipid droplets are tracked using image processing combined with differential interference contrast microscopy, allowing us to determine the position of individual droplets with few-nanometer resolution at 30 frames per second. The trajectories of motion are projected along the microtubule axis, and then a Bayesian statistical approach (see ref. 15) is used to parse the motion into plus-end runs, minus-end runs, and pauses, taking into account the uncertainties in tracking and thermal noise effects (Fig. 4*A*). From this analysis, we extract velocities, lengths of plus-end and minus-end runs, and the frequency and duration of pauses.

With the stochastic model maximally constrained by experiments as discussed above, the predicted motion was quite different from what was observed experimentally: Runs (periods of uninterrupted motion) were very short (Fig. 4*B*), and approximately unidirectional, in contrast to the longer back-and-forth motion experimentally observed (Fig. 4*A*). Further, the predicted motion spent much more time paused than what was observed experimentally [Table 1, third (ST, 5 K ~ 5 D, NoTuning) row].

Because the completely constrained model failed, we considered variants by relaxing specific constraints. We started by adjusting the motors' on rates, which could be somewhat different from their in vitro values, because of the presence of proteins such as dynactin and the microtubule-associated proteins present in vivo but absent in vitro. The "untuned" case initially investigated exhibited excessive interruption from opposite motors, so we decreased on rates to decrease the frequency of potential tugs-of-war, until we matched the mean values of the wild-type run-length and velocity data reasonably well with the simulations [Table 1, fourth (ST, 5 K ~ 5 D, EXPT, WT) row]. However, the rate-adjusted model did not capture certain features. Experimentally [Table 1, first (Experiment, WT, N) row], in the wild type, droplets spend about 24% of the time paused, but in the stochastic simulation with $N = 5$ motors of each type, pauses were still too frequent, and motion was predicted to be paused 48% of the time. Because our experiments are quite reproducible, and the experimental variation is only a few percent, this theoretical prediction was considered to deviate significantly from reality. Furthermore, the stalls were too long, predicted to be about 0.68 ± 0.02 s vs. the experimentally observed pauses with a duration of 0.5 ± 0.003 s.

In addition to the incorrect pausing frequency and duration, the distribution of run lengths was not completely correct. Experimentally, the distribution of bidirectional runs is frequently described by the sum of two decaying exponentials (16), and our Bayesian analysis (15) previously determined that this is a real feature of the underlying motion and not an artifact due to thermal noise or other uncertainties. Indeed, our wild-type experimental data is described by such a distribution (*SI Text*), as were the simulated runs in the minus-end direction, but this was not true for the plus-end simulated data, which can be fit by a single decaying exponential (*SI Text*).

Given these discrepancies, we considered other possibilities. Stall durations were too long, so we decreased the total motor number, N, present on the droplets. This would be consistent with the observation that the pauses were too frequent [compare "time between pauses," in first (Experiment, WT, N) row to fourth (ST, 5 K ~ 5 D, EXPT, WT) row in Table 1), because we hypothesized that pauses occurred when there is a tug-of-war between opposite motors, and the larger the N, the larger the probability of such a tug-of-war occurring. Stall forces measured experimentally suggest that a maximum of $N = 5$ motors are engaged, but many times only a few motors were instantaneously active; perhaps most droplets are moved by fewer than five motors. We therefore considered a stochastic model with $N = 2.5$ motors, that is a mixed population where 50% of the droplets had $N = 3$ motors, and the others had $N = 2$ motors (a choice lower than $N = 2.5$ would be clearly inconsistent with experiments). We adjusted on rates and velocities to match wild-type observations. Results were somewhat better [Table 1, sixth (ST, 2.5 K ~ 2.5 D, EXPT, WT) row]: The percentage of time paused was 26%, consistent with the experimental value of 24%, and time between pauses was reasonable. Further, approximately 65% of the reversals in travel direction were rapid (with no obvious pause between), consistent with the experimental observation of 65%. The mean run lengths and velocities were also acceptable.

The stochastic model with $N = 2.5$ was thus considerably better than the $N = 5$ case, though there was still a discrepancy with the actual experimental data, in that the pause duration was now too short (Table 1). Interestingly, the distribution of plus-end run lengths was now appropriately modeled by a double-decaying exponential distribution (*SI Text*), though the contribution of the fast-decay component was small; the minus-end runs were still reasonably modeled by such a distribution (*SI Text*).

Table 1. Table of run length and pause behavior

Parameter characterized	% duration paused	Time between pauses, s	% of quick reversal, out of run segments	Pause duration, s	Positive run length, nm (skip pause)	Negative run length, nm (skip pause)
Experiment, WT, *N*	24%	3.57	65%	0.524 ± 0.003	558 ± 21	431 ± 21
Experiment, KHC, *N*/2	21%	3.89	63%	0.518 ± 0.004	695 ± 23	588 ± 24
ST, 5 K ~ 5 D, NoTuning	85%	1.78	16%	1.298 ± 0.024	365 ± 14	104 ± 3
ST, 5 K ~ 5 D, EXPT, WT	48%	2.03	45%	0.679 ± 0.020	550 ± 15	395 ± 15
ST, 2.5 K ~ 2.5 D, EXPT, Mut	29%	2.59	59%	0.478 ± 0.013	639 ± 27	486 ± 30
ST, 2.5 K ~ 2.5 D, EXPT, WT	26%	3.03	65%	0.445 ± 0.005	581 ± 19	473 ± 23
ST, 1.5 K ~ 1.5 D, EXPT, Mut	13%	4.74	77%	0.383 ± 0.009	585 ± 27	570 ± 40
ST, 5 K ~ 5 D, EXPN, WT	3%	15.68	95%	0.213 ± 0.006	584 ± 14	436 ± 15
ST, 2.5 K ~ 2.5 D, EXPN, Mut	2%	17.17	94%	0.185 ± 0.019	652 ± 25	494 ± 29
ST, 3 K ~ 12 D, EXPT, WT	38%	2.38	54%	0.502 ± 0.004	540 ± 15	417 ± 16
ST, 1.5 K ~ 6 D, EXPT, Mut	23%	3.01	65%	0.360 ± 0.005	599 ± 22	554 ± 35
MF, 5 K ~ 5 D, EXPT, WT	48%	1.6	5%	0.770 ± 0.009	530 ± 10	420 ± 19
MF, 2.5 K ~ 2.5 D, EXPT, Mut	56%	1.84	4%	1.043 ± 0.021	597 ± 21	478 ± 29
MF, 5 K ~ 5 D, EXPN, WT	10%	4.06	15%	0.403 ± 0.002	583 ± 5	452 ± 5
MF, 2.5 K ~ 2.5 D, EXPN, Mut	14%	2.84	19%	0.390 ± 0.004	367 ± 5	402 ± 6

The tug-of-war process involves competition between opposite motors and results in pauses in motion if this competition is not immediately resolved. The pause kinetics thus provides quantitation of tugs-of-war, so we focus on them both experimentally and theoretically. In several cases, two adjacent rows are related to each other. For instance, the experimental characterization of motion in the wild type is in the first row, and the experimental characterization of motion in the mutant background where there is half as much kinesin is in the second row. Similarly, the fourth row shows the prediction from the stochastic (ST) model for five kinesins (5 K) vs. five dyneins (5 D), with experimental detachment kinetics (EXPT), tuned to match the experimental data by adjusting the motors' on rates. Then, the fifth row is the prediction of the same model, with the same parameters and no tuning, with only the number of motors present changed to be $N = 2.5$ motors. The only unpaired row is row 3, which represents the stochastic model's prediction when completely constrained to use in vitro parameters. EXPN, exponential detachment kinetics.

Critical Test of the Stochastic Theory: Prediction of Motion in a Decreased Kinesin Heavy Chain (KHC) Background. Many aspects of this $N = 2.5$ version of the stochastic model [Table 1, sixth (ST, 2.5 K ~ 2.5 D, EXPT, WT) row] were acceptable, so we tested it further. A good way to test a theory is to fix unknown parameters by fitting experimental data under one in vivo condition, and then use the theory (with fixed parameters) to predict what should occur in a second in vivo condition where any changes in parameters are known/measured a priori [see, e.g., the prediction of lysosomal run lengths in neurons, as affected by decreasing dynein processivity (13)]. Here, we took such an approach. Using a kinesin-null mutation KHC-27 (which makes no protein), we created embryos from KHC-27/+ mothers, that is, mothers that had one null and one wild-type copy of the gene (14). In this background, lipid droplets are moved by 50% less kinesin (as determined by biochemistry, measuring droplet-bound kinesin, and by force measurements, assessing the number of active motors) (14). Thus, by construction, instead of $N = 2.5$, in this new background $N \approx 1.25$; for simplicity (and also to match experimental constraints, which clearly indicate significant contribution from a second motor in the mutant case), we modeled this theoretically using an equal combination of $N = 1$ and $N = 2$ droplets. Force measurements indicate that the number of active dynein motors was also decreased by 50% (14); such feedback is common, and has been observed in a number of systems (17), although its mechanistic underpinnings are unknown. We looked at the same developmental phase as for the wild-type embryos, so we used the same values of all the adjustable parameters that we fixed by fitting the wild-type motion. With these constraints, there are no adjustable parameters.

In this test, the stochastic $N = 1.5$ theory [Table 1, seventh (ST, 1.5 K ~ 1.5 D, EXPT, Mut) row] failed to correctly reproduce the experimental observations in a number of qualitative as well as quantitative ways. First, the stochastic model simulations predicted that the percentage of time paused decreased (from 26% to 13%). This was theoretically expected (given the pause frequency differences between the $N = 5$ and $N = 2.5$ simulations, and see discussion in *SI Text*), but not what was observed experimentally, where total time paused was approximately constant within experimental error [24% vs 21%; Table 1, first (Experiment, WT, N) row vs. second (Experiment, KHC, $N/2$) row]. Similarly, theoretically, the time between pauses increased dramatically [Table 1, seventh (ST, 1.5 K ~ 1.5 D, EXPT, Mut) row vs. sixth (ST, 2.5 K ~ 2.5 D, EXPT, WT) row], and pause duration decreased, because of fewer engaged motors, but this was not observed experimentally. Finally, experimentally, the decrease in N resulted in longer run lengths in both directions, but in theory, the effect was not observed in the plus-end direction, and the predicted increase in minus-end run length (21%) was smaller than observed (36%). Thus, although some of the model predictions were qualitatively in agreement with the experimental data (e.g., the predicted increase in velocities in each direction), some were not (pause frequencies and durations, and plus-end run lengths increasing), and even those that had a correct trend had magnitudes that were not consistent with experiments. We conclude that although the stochastic tug-of-war model with actual in vitro detachment kinetics and in vitro processivities recovers some of the features observed in the wild-type motion, it is not an accurate model of the experimental process.

Additional Variants. Overall, we considered relaxing a number of other constraints, including adjusting single-motor processivity, trying exponential instead of experimentally measured detachment kinetics, and allowing uneven numbers of motors (see *SI Text* for details). We also investigated mean-field tug-of-war models in addition to the stochastic models (see *SI Text*). None of these variants correctly described the data (see *SI Text* and Table 1).

Discussion

Experimental Measurements and Their Ramifications. Our recent NudE/Lis1 studies (9) highlight the importance of single-motor detachment kinetics for ensemble function under load; such kinetics are expected to be of particular importance in determining outcomes of hypothetical tugs-of-war between groups of motors. We systematically measured both kinesin and dynein detachment kinetics in vitro, and found neither as expected. Dynein had "catch-bond" detachment kinetics, with its detachment rate decreasing with increasing load. This could, in principle, contribute to dynein being able to serve as an "anchor" to hold subcellular organelles in place (18) under high load. We expect that these characterizations of the motors' detachment kinetics will be useful for theoretical models describing how ensembles of motors function together. We constrained two classes of models—stochastic and mean-field—by these data and compared their predictions to ensemble motor behavior in vitro. The stochastic model describes the in vitro data reasonably well, but the mean-field theory model does not.

Tug-of-War Scenarios to Explain Bidirectional Motion. Many cargos move bidirectionally, reversing travel direction every few seconds. The key determinant in net, or average transport, is the duration of runs (periods of travel between reversals) in each direction. Because run length is determined by reversal frequency, it is important to understand the reversal process. Tug-of-war models are appealing because they suggest that the reversals reflect unregulated (stochastic and mechanical) competitions between opposite-polarity motors on the cargo (a group of plus-end kinesins and a group of minus-end dyneins), allowing us, in principle, to use single-motor properties measured in vitro to predict and understand emergent transport in vivo.

We evaluated such models critically, within the context of lipid-droplet (LD) motion in *Drosophila* embryos, using a strategy previously used studying multiple dynein motors in vivo, in cultured neurons. We constrained the models' "free" parameters as much as possible via experimental data and then determined the values of any unconstrained parameters by fitting the theory's predictions to one experimental set of in vivo (wild-type) data. Once the theory's parameters were fixed, it was used to predict the outcome of a known change, with no further adjustment. In the previous study, modeling essentially unidirectional transport (13), the "known change" was a (in vitro measured) reduction in single-motor processivity, caused by the dynein Loa mutation. Here, the known change was the reduction in the total motor number N on the cargo. In the dynein Loa study we achieved quantitative agreement between theory and experiment, but here, for bidirectional transport, we were unable to do so. Thus, we conclude that although tugs-of-war likely exist some of the time, using this mechanism alone one cannot explain bidirectional motion—there must be an additional mechanism (likely enzymatic) that contributes to regulation of the motors.

One could wonder about whether we failed to find the right choice of parameters, but specific qualitative discrepancies between the theoretical predictions and experimental observations (discussed below) suggest to us that this is unlikely.

The Importance of Pauses. In a tug-of-war model, pauses occur when the opposite motors "battle," and as such are a crucial readout, sensitive to the tug-of-war process. The frequency of pauses is determined by a combination of the number of motors present on the cargos, and the on rates of those motors. The pause durations are determined both by the number of motors engaged in the tug-of-war, the individual motors' on rates, and the detachment kinetics of the motors under load. One key feature of tug-of-war models is that the more motors are present, the more opportunities for battles one has, and thus the higher the frequency of pauses. This was true for almost all variants of the tug-

of-war models we examined, but not observed experimentally. The only exception to this occurs when the motors detach easily (some exponential-detachment models), so that the majority of pauses are so short that they are undetected. In this case, pause frequency may be less affected by the number of motors present, but pause duration will be extremely short. A second qualitative feature of pauses/tug-of-war models is that more motors frequently lead to longer pauses; this can be seen experimentally in vitro in the detachment studies (Fig. 2). However, this change in pause duration is also not experimentally observed in the lipid-droplet system when the number of motors is altered.

The Relationship Between Run Lengths and the Number of Motors Present. For unregulated unidirectional motors, more motors move further (6, 12). If detachment kinetics of the motors are sufficiently fast above stall (e.g., in some variants of the exponential detachment models), this is also true for bidirectional models, because, e.g., one dynein motor stochastically attaching to oppose three kinesin motors is quickly overwhelmed and releases before there is a significant chance for additional dynein motors to bind and help it sustain the competition. However, for actual single-motor detachment kinetics (measured in vitro), the motors' off rates under load are slow enough that when a single motor stochastically attaches to oppose a group of opposite-polarity motors moving the cargo, it is able to "hold on" for a time comparable (or longer than) the typical on time of its compatriots. In this case, a stochastic attachment event from a single motor has a high probability of turning into a full-out tug-of-war between approximately evenly matched sets of opposite motors, and thus can cause a reversal. Then, for otherwise fixed parameters, the more motors present, the more tugs-of-war, and the shorter the travel of the cargo between pauses or reversals.

Qualitative Mismatch Between Theory and Experiments. Overall, as discussed above, in tug-of-war scenarios, for fixed parameter values, more motors lead to more frequent tugs-of-war, as long as a single motor can successfully (at least temporarily) pause a group of opposite-polarity motors. This occurs when the motors' detachment kinetics are not exponential above stall. Hence, in the models, more motors imply more pauses. Further, in the models, and confirmed in vitro, more motors tend to lead to longer pauses. We tested both these general properties in vivo, by comparing motion in wild-type embryos to motion in embryos with reduced kinesin on the LDs [reduced LD kinesin reduces number of engaged motors (14)]. Our analysis of motion in these two backgrounds shows that reduced motors did not lead to a decrease in pause frequency, nor a change in pause duration. Thus, in addition to quantitatively not matching the experimental data, the general trend predicted by the tug-of-war models is not observed in our experiments.

In any theoretical investigation, one makes simplifications. If a theory fails, one might question the simplifications, or whether the wrong parameter set was chosen, rather than concluding the theory is fundamentally wrong. Here, we ignore potential effects of NudE/Lis1 to decrease dynein's detachment under load (9). Whether this specific effect on dynein's motor output contributes to bidirectional transport is unclear, but if so, the effect would be to make the models even worse: Tugs-of-war would be more severe, and pauses would be even longer. In the most likely variants of the models, motion is already predicted to spend too much time paused.

The mean-field models have other difficulties. The stochastic models are better in vitro; the justification for ignoring this, and believing that the mean-field models will suddenly do better in vivo, is unclear. Further, our experiments clearly constrain the number of motors per wild-type droplet to between $N = 2.5$ and $N = 5$, and over this range pausing predictions are dramatically wrong: With real detachment kinetics, cargos spend twice as much time paused as they ought to, and for exponential detachment kinetics, they spend only half as much time paused.

Conclusion

As studied, neither the stochastic nor mean-field tug-of-war models describe our observations, and the difference in qualitative trends (see above) support the notion that slightly different choices of parameter values is unlikely to be better. Conceivably, there could be unknown/unconsidered factors that exist in vivo that very significantly modulate the properties of the motors (and the outcomes of tugs-of-war) in ways that we have not considered. Thus, although we favor the hypothesis that a significant portion of lipid-droplet directional switching does not result from unregulated tugs-of-war, this hypothesis should be revisited as new motor regulators are discovered.

In addition to providing strong indication that the tug-of-war picture is insufficient to capture all aspects of transport dynamics in vivo, our work provides a convenient template for future evaluations of the correspondence between tug-of-war models and experimental observations. Further studies across different motor species and in different in vivo environments should allow increasingly better understanding of the limits of tug-of-war models.

Methods

Quantitation of lipid-droplet motion was as described in ref. 14, and optical-trapping assays, data recording, particle tracking, and stalling-force analysis were performed as described in refs. 6 and 12. Theoretical modeling was done as described in ref. 8, with modifications described above. Further methods details are in the *SI Text*.

ACKNOWLEDGMENTS. We gratefully acknowledge dynein from Dr. Richard Vallee (Columbia University, New York, NY). Work done at the University of California, Irvine, was supported by National Institutes of Health/National Institute of General Medical Sciences Grant GM064624 to S.P.G. and GM079156 to C.C.Y. and S.P.G. Work done at the University of California; Davis, was supported by National Institutes of Health/National Institute of General Medical Sciences Grant GM068952 to A.M.

1. Gross SP (2004) Hither and yon: A review of bi-directional microtubule-based transport. *Phys Biol* 1:R1–R11.
2. Muller MJ, Klumpp S, Lipowsky R (2008) Tug-of-war as a cooperative mechanism for bidirectional cargo transport by molecular motors. *Proc Natl Acad Sci USA* 105:4609–4614.
3. Soppina V, Rai AK, Ramaiya AJ, Barak P, Mallik R (2009) Tug-of-war between dissimilar teams of microtubule motors regulates transport and fission of endosomes. *Proc Natl Acad Sci USA* 106:19381–19386.
4. Hendricks AG, et al. (2010) Motor coordination via a tug-of-war mechanism drives bidirectional vesicle transport. *Curr Biol* 20:697–702.
5. Gross SP, et al. (2000) Dynein-mediated cargo transport *in vivo*. A switch controls travel distance. *J Cell Biol* 148:945–956.
6. Vershinin M, Carter BC, Razafsky DS, King SJ, Gross SP (2007) Multiple-motor based transport and its regulation by Tau. *Proc Natl Acad Sci USA* 104:87–92.
7. Klumpp S, Lipowsky R (2005) Cooperative cargo transport by several molecular motors. *Proc Natl Acad Sci USA* 102:17284–17289.
8. Kunwar A, Vershinin M, Xu J, Gross SP (2008) Stepping, strain gating, and an unexpected force-velocity curve for multiple-motor-based transport. *Curr Biol* 18:1173–1183.
9. McKenney RJ, Vershinin M, Kunwar A, Vallee RB, Gross SP (2010) LIS1 and NudE induce a persistent dynein force-producing state. *Cell* 141:304–314.
10. Coppin CM, et al. (1997) The load dependence of kinesin's mechanical cycle. *Proc Natl Acad Sci USA* 94:8539–8544.
11. Carter NJ, Cross RA (2005) Mechanics of the kinesin step. *Nature* 435:308–312.
12. Mallik R, Petrov D, Lex SA, King SJ, Gross SP (2005) Building complexity: An in vitro study of cytoplasmic dynein with in vivo implications. *Curr Biol* 15:2075–2085.
13. Ori-McKenney KM, et al. (2010) A cytoplasmic dynein tail mutation impairs motor processivity. *Nat Cell Biol* 12:1228–1234.
14. Shubeita GT, et al. (2008) Consequences of motor copy number on the intracellular transport of kinesin-1-driven lipid droplets. *Cell* 135:1098–1107.
15. Petrov DY, et al. (2007) Studying molecular motor-based cargo transport: What is real and what is noise? *Biophys J* 92:2953–2963.
16. Gross SP, et al. (2002) Interactions and regulation of molecular motors in Xenopus melanophores. *J Cell Biol* 156:855–865.
17. Ally S, Larson AG, Barlan K, Rice SE, Gelfand VI (2009) Opposite-polarity motors activate one another to trigger cargo transport in live cells. *J Cell Biol* 187:1071–1082.
18. Ligon LA, Holzbaur EL (2007) Microtubules tethered at epithelial cell junctions by dynein facilitate efficient junction assembly. *Traffic* 8:808–819.

Supporting Information

Kunwar et al. 10.1073/pnas.1107841108

SI Text

Details of Detachment Studies. To measure the off rates more systematically, we used an optical trap–based method. Kinesin or dynein were attached to polystyrene beads, but in limited amounts, so that approximately one of every three beads bound and moved, making sure that we were in the single-motor regime. We then applied the following automated approach. First, the bead was brought into contact with the microtubule, and its position in the optical trap was detected using the quadrant photodiode. For the subset of beads with active motors, when the motor attached to, and started walking along, the microtubule, it moved the bead toward the edge of the optical trap. When the bead reached a predefined location (typically 100 nm for kinesin, and 70 nm for dynein, from the trap center), our automated software increased the laser power, so that the motor was suddenly under a "superforce" situation; the magnitude of the superforce was determined by how much power was used. We then measured the time to detachment (i.e., the time between when the laser power was increased and the moment when the motor detached from the microtubule, allowing the bead to fall back rapidly toward the trap center). Examples of such events are shown in Fig. 2*A* for kinesin and Fig. 2*B* for dynein. By fitting a single decaying exponential function to such distributions, we extracted a characteristic off rate for each superforce value, summarized for different applied superforces in Fig. 2*E* for kinesin and Fig. 2*F* for dynein.

Performance of Unidirectional Stochastic vs. Mean-Field Model Under Load. We previously suggested that because of uneven load sharing (1), the stochastic model had improved ensemble performance under load. However, at that time the two models had different superforce assumptions. Now, more appropriately, we compare models with identical parameter values and superforce behavior. Consistent with the previous suggestion, we find that binding events even below stall last longer for the stochastic model (Fig. S1*A*) than for the mean-field model, with the difference increasing as one goes to higher loads. Runs are a bit more confusing: The mean-field model predicts slightly longer runs than for the stochastic model (Fig. S1 *B* and *C*), but this actually reflects the fact that the stochastic model allows brief backward "blips" of motion of the cargo because of detachment of the lead motor, whereas the mean-field model does not consider the possibility that motors could be ahead or behind each other. When corrected for the blips, the stochastic run lengths are longer, consistent with the longer binding times (Fig. S1 *B* and *C*, arrow marked) Note that the superstall behavior we implement, based on the experimental measurements, dramatically improves the ensemble behavior when compared with the use of exponential detachment kinetics above stall (as originally assumed by Klumpp et al. (2) (compare MF, EXPN in Fig S9*A* to MF, EXPT in Fig S9*C*). Specifically, the exponential detachment assumption makes the ensemble very sensitive to applied load (Fig. S1 *B* and *C* showing predicted run lengths), and thus the group of motors detaches quickly. Obviously, a mean-field prediction with this kind of detachment is even further from actual experiments (compare MF, EXPN in Fig S9*A* to MF, EXPT in Fig S9*C*). In conclusion, constrained by single-molecule data, the stochastic model appears to describe ensemble behavior in vitro reasonably well, whereas neither version of the mean-field theory is as accurate.

Variants of the Stochastic Model: Lower Processivity. Because relaxing the on rate and motor number constraint failed, we considered relaxing further constraints. Although some studies suggest that single-motor kinesin processivity is the same in vivo as in vitro (3), we considered the possibility that here it was lower. We therefore looked at a stochastic model with $N = 5$ motors, where both kinesin and dynein processivities were chosen to be approximately 500 nm. As for the long-processivity $N = 5$ case above, droplets spent too much time paused (39% vs. the experimental 24%), so this model was rejected. We thus again considered the possibility of the wild type being described by $N = 2.5$ motors. As for the long-processivity case above, by tuning on rates appropriately, this was again close enough that it reasonably matched the wild-type experimental data. We thus examined predictions for the kinesin heavy chain 27/+ embryos, modeled using the same parameters as the wild type, but now choosing $N = 1.5$. Similar to the longer processivities $N = 1.5$ case, this was closer to experimental data, but still unacceptable. In particular, there was still the qualitative problem that the percentage of time stalled decreased (from 23% to 15%), whereas experimentally they did not, and although the plus-end and minus-end run lengths did increase, the magnitude of the effect (between 4% and 12%) was much smaller than observed experimentally (between 25% and 36%). Thus, we conclude that neither the $N = 5$ nor $N = 2.5$ stochastic tug-of-war models with in vitro superstall behavior are acceptable, regardless of the choice of on rates or single-motor processivities.

Variants of the Stochastic Model: Exponential Detachment Kinetics. In principle, there could also be factors in vivo that alter single-motor detachment kinetics. Others have suggested that tug-of-war models correctly reproduce the data, when exponential detachment kinetics are assumed (4), so we considered them with the $N = 5$ stochastic model (Fig. 4*D*). Because the motors detach much more readily under load, exponential detachment kinetics makes pauses less likely, and when we tuned the motors' on rates to reproduce the observed run lengths, we observe very few pauses [3% of time paused vs. the experimentally observed 24%; Table 1, eighth (ST, 5 K ~ 5 D, EXPN, WT) row], and the time between pauses was extremely long. The predicted mean pause duration (0.21 ± 0.006 s) was much shorter than that observed experimentally (0.52 ± 0.003 s). Again, the increase in run lengths with decreasing number of motors present (Table 1) is significantly smaller than that observed experimentally.

Variants of the Stochastic Model: Uneven Numbers of Motors. Our experimental measurements indicate that overall stall forces in each direction are approximately balanced, and suggest that the single-motor stall force is approximately 2.5 pN. In principle, one could get such a force of approximately 2.5 pN from approximately two dynein motors, though it is unclear how such a force would come about from kinesin functioning with in vitro properties. Nonetheless, because others have modeled bidirectional transport assuming uneven numbers of motors (5), we considered the case of the wild-type lipid droplet with three kinesin motors functioning with in vitro (approximately 5 pN) stall forces, opposed by 12 dynein motors with in vitro (1.25 pN) stall forces (chosen to balance forces, because this is observed experimentally). We assumed experimental in vitro detachment kinetics and single-molecule processivities, and tuned the on rates of the motors, in order to match mean experimental run lengths for

the wild type. When we matched run lengths, droplets spent too much time paused (38%), though the durations were acceptable [Table 1, tenth (ST, 3 K ~ 12 D, EXPT, WT) and eleventh (ST, 1.5 K ~ 6 D, EXPT, Mut) rows]. Further, quantitatively, the $N/2$ case did not correctly predict the experimentally observed changes in run lengths, and was qualitatively incorrect in predicting decreased frequency of pausing, and shorter pause durations, both of which were not observed experimentally.

Comparing in Vivo Experimental Data to the Mean-Field Bidirectional Model. Because of its more accurate predictions of ensemble function in vitro, the stochastic model had been our preferred model to investigate the tug-of-war hypothesis in vivo. Because it failed, regardless of which experimental constraints were relaxed, and because in vivo there could, in principle, be a physical linkage resulting in motors approximately equally sharing load, we also evaluated the mean-field tug-of-war model previously reported to explain lipid-droplet motion (4). The original model assumed exponential detachment kinetics for the motors, so we started by investigating this. That is, we relaxed both the constraint on detachment kinetics and on rates, and tuned on rates by fitting the wild-type data, and then looked at how well the model predicted motion in the kinesin-mutant background. The wild-type fit was acceptable as far as run lengths [Table 1, fourteenth (MF, 5 K ~ 5 D, EXPN, WT) row], but pause durations were too short, and the percentage of time paused was too little. Further, the prediction for the mutant background was quite far off [Table 1, fifteenth (MF, 2.5 K ~ 2.5 D, EXPN, Mut) row] both quantitatively and qualitatively: Run lengths were predicted to go down in the mutant, whereas in fact experimentally they increased, and in fact the model predicts a loss in net plus-end transport, though one does not occur experimentally. Time between pauses was predicted to go down, which was also incorrect. We therefore incorporated the experimental superstall behavior into the mean-field theory [Table 1, twelfth (MF, 5 K ~ 5 D, EXPT, WT) and thirteenth (MF, 2.5 K ~ 2.5 D, EXPT, Mut) rows]. In this case, again, the wild-type fit is acceptable, but here, pauses are too frequent, last too long, and overall the predicted amount of time paused is much more than what is observed experimentally (Table 1).

Other Factors Relevant for Models of Bidirectional Transport. We considered both stochastic and mean-field tug-of-war models, and we concluded that they are inadequate. This supports the general hypothesis that some significant portion of lipid-droplet directional switching does not simply result from unregulated tugs-of-war, but instead reflects additional factors that actively engage or disengage motors, regulating reversals, and perhaps pauses. In principle, a number of molecular interactions are implicated in this control. First, past studies on lipid-droplet motion suggest dynactin may contribute to avoiding tugs-of-war (6), a finding supported in other systems (7). Second, more generally, we now have examples of proteins (NudE and Miro) capable of inactivating either dynein or kinesin, respectively (8, 9). Whether these proteins play broad roles in bidirectional transport is unknown. Finally, in some specific bidirectional transport situations, there are clearly feedback mechanisms to regulate motor activity. We observed that a decrease in the number of active kinesin motors moving lipid droplets was correlated with a decrease in the number of active dynein motors (10). A similar observation was made for bidirectional peroxisome motion, where lack of one set of active motors resulted in inactivation of motion in the opposite direction (11). Intriguingly, for the peroxisomes, this inactivation could be rescued by a second type of opposite-polarity motor, not usually present, suggesting the inactivation resulted from lack of force production rather than a specific molecular interaction. In vitro, neither kinesin nor dynein requires externally applied load to be active (12, 13), suggesting that this requirement in vivo reflects the presence of additional as-yet-unknown regulatory factors, perhaps including dynactin. It will be particularly exciting to understand the molecular details of this unexplored regulatory mechanism.

SI Materials and Methods

Protein Purification. Cytoplasmic dynein was purified from wild-type rat brain as described in ref. 8. Full-length *Drosophila* kinesin was purified from the wild-type *Drosophila* embryos as in ref. 14.

Bidirectional Study of Lipid Droplets. Studies of lipid droplets in WT and mutant embryos are as described in ref. 10. Experimental and theoretical trajectories of motion were parsed into segments as in ref. 15. Table parameters were calculated from this analysis.

In Vitro Optical Bead Assay. Optical-trapping motility assays, data recording, particle tracking, and stalling-force analysis were performed as previously described in refs. 12 and 16.

For dynein and kinesin assays, a 489-nm-diameter carboxylated polystyrene bead (PolySciences), with nonspecifically attached motors, was positioned in a flow chamber above a stabilized microtubule for 30 s. The single-motor range was attained when the percentage of beads exhibiting binding events (the motor binds to the microtubule and is processive) is smaller than or equal to 30%. For the run-length measurements of single *Drosophila* kinesin, an individual run was defined as the travel between a bead binding to, and then detaching from, a microtubule (with optical trap turned off). The distribution of kinesin run lengths was fitted to single exponential decay to obtain its mean run length and uncertainty.

Definitions of the Stall Force (F_s) and Detachment Force (F_d) and Their Measurements. We define the stall force (F_s) as the mean value of the load force at which the motor stops moving. For dynein or kinesin stall-force measurements, a trap stiffness of 2.08 or 5.6 pN per 100 nm, respectively, was used. An event was classified as a stall if the bead coated with single-motor moved away from trap center and held its plateau position for ≥500 ms for kinesin, or 100 ms for dynein, before detachment. In order to be counted as a stall, the mean velocity of the bead during the stall was required to be within 10 nm/s of 0 nm/s. The distribution of stall forces was fitted with a Gaussian function, and the fitted Gaussian peak position (and uncertainty) represents the mean stall force (and SEM).

We define the detachment force (F_d) as the characteristic value of the force detaching a single moving motor from the microtubule. The detachment force F_d was defined earlier (2) as $F_d = k_B T/\delta_l$, where $k_B T$ is thermal energy and δ_l is extension of the potential barrier between the attached and detached state of the motor. Equivalently, if the rate of detachment as a function of the load force F is proportional to exponential factor $\mathrm{Exp}(F/F_d)$, as assumed in recent models (17, 18) based on Kramer's theory, then the inverse of the coefficient $1/F_d$ in this factor is the detachment force.

In our case, to experimentally determine the detachment force F_d, we first obtained the distribution of such forces below the stall, by recording the forces at which the motors detached abruptly while moving. These forces were obtained by multiplying the trap stiffness by the distance between the detachment location and the trap center. For dynein and kinesin, a trap stiffness of 2.08 and 5.6 pN per 100 nm, respectively, were used. The distribution of the detachment force is not symmetric, and hence the mean value was obtained using the statistical average of the data.

Superforce Experiments. For the detachment kinetics experiments, we applied the following automated approach: First, the bead was brought into contact with the microtubule, and its position in the

optical trap was detected using the quadrant photodiode. For the subset of beads with active motors, when the motor attached to, and started walking along, the microtubule, it moved the bead toward the edge of the optical trap. When the bead reached a predefined location (typically 100 nm for kinesin, and 70 nm for dynein, from the trap center), our automated software increased the laser power, so that the motor was suddenly under a superforce situation; the magnitude of the superforce was determined by how much power was used. We then measured the time to detachment (i.e., the time between when the laser power was increased and the moment when the motor detached from the microtubule, allowing the bead to fall back rapidly toward the trap center). The distribution of detachment times was fitted to a single exponential decay. The obtained decay constant and uncertainly presented in each plot represent the average detachment time and SEM, respectively. Statistical significance was determined using the Student's t test.

Theoretical Simulations. ***Generalized mean-field models of multiple motor transport. Generalized mean-field model of unidirectional transport.*** Force-velocity relations of single motors can be well approximated by the following mathematical expression:

$$v(F) = v(1 - (F/F_s)^w), \quad \text{[S1]}$$

where v is the unloaded velocity of the single motor, F is the load force, and F_s is the stall force. If the motor moves in steps of length d, then the motor can be described effectively with the load-dependent rate of stepping:

$$k_{\text{step}}(F) = (v/d)[1 - (F/F_s)^w]. \quad \text{[S2]}$$

The force-dissociation relation of a single motor can be written as

$$\varepsilon(F) = \varepsilon\Omega(F), \quad \text{[S3]}$$

where ε is the load-free dissociation rate, and function $\Omega(F)$ determines the load dependence of the detachment-rate. Recent models have assumed function $\Omega(F)$ as exponential function based on Kramer's theory (i.e., $\Omega(F) = \text{Exp}(F/F_d)$, where F_d is the detachment force).

Recent work (17) extended the mean-field model proposed in ref. 18 onto a variety of single-motor force-velocity relations. Importantly, in both refs. 17 and 18, the force-dissociation rate for motors was assumed to be an exponentially increasing function of load, so that $\varepsilon_i(F) = i\varepsilon\text{Exp}(F/iF_d)$, where i is the number of engaged motors. In our generalized model, a cargo particle is transported cooperatively by N molecular motors; out of N, variable number $i(t)$ motors are engaged at any given moment. The engaged motors share the applied load F equally, so the force F/i is applied to each of i engaged motors. Thus, the cargo has the velocity:

$$v_i(F) = \begin{cases} v(1 - (F/iF_s)^w) & \text{for } F \le iF_s \\ 0 & \text{for } F \ge iF_s \end{cases}. \quad \text{[S4]}$$

Here, exponent w determines the linearity/nonlinearity of the force-velocity curve. For $w = 1$, the force-velocity curve is linear and reduces to the case investigated in ref. 18; for $w > 1$, force-velocity curves are superlinear; and for $w < 1$, force-velocity curves are sublinear.

The number of engaged motors increases with the rate

$$\pi_i = (N - i)\pi \quad \text{[S5]}$$

and decreases with the rate

$$\varepsilon_i(F) = i\varepsilon\Omega(F/i), \quad \text{[S6]}$$

where π is the attachment rate of a single motor, ε is the detachment rate of unloaded single motor, and N is the total motor number on the cargo. The new feature of the mode is the force dependence of the dissociation rate of a single motor is given by function Ω, which can, in principle, have many different functional forms.

We use the stationary solutions of the master equation obtained in ref. 18 expressing the probability for the system to have i engaged motors in terms of the motor parameters,

$$P_0 = \left[1 + \sum_{i=0}^{N-1}\prod_{j=0}^{i}\frac{\pi_j}{\varepsilon_{j+1}}\right]^{-1} \quad \text{and} \quad P_i = P_0\prod_{j=0}^{i-1}\frac{\pi_j}{\varepsilon_{j+i}}, \quad \text{[S7]}$$

to find the average velocity of the cargo,

$$V = \sum_{i=1}^{N} v_i\frac{P_i}{1 - P_0}, \quad \text{[S8]}$$

and average run length of the cargo,

$$X = 1 + \sum_{i=1}^{N-1}\prod_{j=1}^{i}\frac{v_{j+1}\pi_j}{v_j\varepsilon_{j+1}}. \quad \text{[S9]}$$

For $w = 1$ and $\Omega(F) = \text{Exp}(F/F_d)$ for any F, the model is identical to the one proposed in ref. 18. For kinesin motors, we use $w = 2$, and for dynein motors we use $w = 1/2$ in the force-velocity relations, unless otherwise stated.

The average detachment time of cargo can be obtained from a simple argument that in the stationary state effective unbinding rate of cargo from any one of the attached state is equal to the effective binding rate of an unattached cargo. The resulting expression is given by (18):

$$T_{1,N} = \frac{1}{\varepsilon_1}\left(1 + \sum_{i=1}^{N-1}\prod_{n=1}^{i}\frac{\pi_n}{\varepsilon_{n+1}}\right). \quad \text{[S10]}$$

Generalized mean-field model of bidirectional transport. To study the bidirectional transport, Muller et. al. (4), developed a model of bidirectional cargo transport in which N_+ plus-directed and N_- minus-directed motors attach and detach from a microtubule stochastically with given on and off rates. The bidirectional model is an extension of the model of unidirectional transport (18). The force-velocity relation for the motors was assumed to be a linear function of the applied load, and force-dissociation rate of the motors was assumed to be an exponentially increasing function of the load. When bound to the microtubule, the motor walks forward with the velocity v_F, which decreases linearly with the external force and reaches zero at the stall force F_s. Under superstall external forces ($F > F_s$), the motor walks backward slowly with backward velocity v_B

$$v(F) = \begin{cases} v_F(1 - F/F_s) & \text{for } F \le F_s \\ v_B(1 - F/F_s) & \text{for } F \ge F_s \end{cases}. \quad \text{[S11]}$$

The rates for unbinding of one of the bound motors and for binding of an additional motor on the cargo are found based on the assumption that (i) the presence of opposing motors induces a load force, and (ii) each plus motor feels the load F_+ (and generates the force $-F_+$), and each minus motor feels the load $-F_-$ (and generates the force F_-); this means that the force

balance on a cargo pulled by n_+ plus and n_- minus motors is given by

$$n_+F_+ = -n_-F_- = F_c. \quad \textbf{[S12]}$$

The sign of the force was chosen positive if a load was on the plus-directed motors (i.e., if the force pointed into the minus direction).

The effective unbinding rate for the plus-directed motor is

$$n_+\varepsilon_+ \exp[F_c/(n_+F_{d+})], \quad \textbf{[S13]}$$

and the effective rate for the binding of one plus-directed motor is

$$(N_+ - n_+)\pi_+. \quad \textbf{[S14]}$$

Above and hereafter, the index "+" labels the plus-directed motors properties and index "−" labels the minus-directed motors properties.

The cargo force F_c is determined by the condition that the plus-directed motors, which experience the force F_c/n_+, and the minus-directed motors, which experience the force $-F_c/n_-$, move with the same velocity, which is the cargo velocity v_c:

$$v_c(n_+,n_-) = v_+(F_c/n_+) = -v_-(-F_c/n_-). \quad \textbf{[S15]}$$

Here, the sign of the velocity is taken positive in the plus direction and negative in the minus direction.

In the case of stronger plus-directed motors, $n_+F_{s+} > n_-F_{s-}$, the cargo force and velocity are given by the expressions

$$F_c(n_+,n_-) = \lambda n_+F_{s+} + (1-\lambda)n_-F_{s-} \quad \textbf{[S16]}$$

and

$$v_c(n_+,n_-) = [n_+F_{s+} - n_-F_{s-}]/[(n_+F_{s+}/v_{F+}) + (n_-F_{s-}/v_{B-})]. \quad \textbf{[S17]}$$

Here, λ is given by

$$\lambda = 1/[1 + (n_+F_{s+}v_{B-}/n_-F_{s-}v_{F+})]. \quad \textbf{[S18]}$$

In this case, the cargo moves to the plus direction with velocity $v_c > 0$. In the opposite case of the stronger minus-directed motors (i.e., $n_+F_{s+} < n_-F_{s-}$), in Eqs. **S16** and **S17**, the plus-directed motor forward velocity v_{F+} has to be replaced by its backward velocity v_{B+}, and the minus motor backward velocity v_{B-} has to be replaced by its forward velocity v_{F-}. The cargo moves into the minus direction: $v_c < 0$.

In order to obtain run lengths and run velocities, individual cargo trajectories were generated using the Gillespie algorithm for the motor attachment/detachment kinetics, and cargo was allowed to move with the velocity v_c in the intervals between the attachment/detachment events.

In order to generalize this model, we use the generalized form of force-velocity relations in Eq. **S11** (i.e., Eq. **S1**). We use a superlinear-force-velocity relation ($w = 2$) for kinesin motors and a sublinear-force-velocity relation ($w = 1/2$) for dynein motors, unless otherwise stated. In addition, we also use detachment kinetics given by function Ω instead of a purely exponential detachment kinetics. Function Ω is obtained from the experimentally constrained detachment kinetics of kinesin and dynein motors as above. The analysis of the simulated trajectories was performed using the criteria given for runs and pauses in ref. 4.

Stochastic model of multiple motor transport. Stochastic model of unidirectional transport. To model the multiple motor transport, we place N motors on the cargo, so that motor heads are attached to a single spot by elastic linkages. According to recent measurements (19), the linkage between the motor domain and the bead is highly nonlinear: when stretched beyond the rest length, it behaves as a relatively stiff linear spring characterized by the spring constant ∼0.32 pN/nm (1). However, its effective compressional rigidity is very low, ∼0.05 pN/nm, i.e. the link buckles almost without resistance when compressed (19). Thus, we model each linkage as a linear spring exerting restoring force when stretched beyond the rest length and not generating any force if the distance between the bead attachment point and the motor heads is less than the rest length. The model is one dimensional, so all distances are measured along the motors' track. In the simulations, we use the appropriate values of linkage stiffness and rest lengths for kinesin and dynein. Each dissociated motor binds to the track with the constant on rate, and each engaged motor detaches with the rate given by Eq. **S3** dependent on the instantaneous force applied to this motor head by the elastic link. Each motor makes a forward step with the force-dependent rate Eq. **S2**. Probabilities of binding, unbinding and stepping events are computed by multiplying the respective rate by the time step. The instantaneous position of the cargo is calculated at each step from the requirement that the total force on the cargo from the load and all elastic links is equal to zero in absence of thermal noise and viscosity of the medium.

Simulation of the single motor. We use the Monte Carlo procedure (1, and 20) to update the state (position and engaged or detached state) in increments of the time step Δt. The time step Δt is chosen to be sufficiently smaller than the fastest characteristic time (in our case, detachment of the last attached motor under a high load). We used $\Delta t = 10^{-6}$ s that conforms with this requirement.

The computational procedure is as follows.

1. Initial condition: At $t = 0$, $x = 0$, where x is the position of the motor on the track.
2. Updating procedure: Repeat the following steps up to t_{max} in increments of Δt.

i. If $t > t_{max}$ go to step 3.
ii. Detachment: Calculate $P_{off} = \varepsilon(F) * \Delta t$. First try detachment with the probability P_{off}. If the detachment occurs, go to step 3, else go to step (iii).
iii. Stepping: If the motor remains attached after step (ii), stepping occurs with probability $P_{step} = k_{step}(F) * \Delta t$. After stepping, x is changed to $x + d$, where $d = 8$ nm.

3. Run length is the current value of x. Velocity is obtained by dividing the current position x by the current time t.

Simulation of the multiple motors. We put N motors on the cargo, so that the motor heads are attached to the cargo via the linkage of the rest length l. Each linkage exerts a restoring force when stretched beyond their rest length. The linkages have no compressional rigidity (i.e., they exert no force when compressed). Initially, we place the bead's center of mass at the origin and allow all motors to attach to any discrete binding site on the track within distance l on either side of the bead. Once the motors are attached, we calculate the initial position of the bead's center of mass so that the sum of all elastic forces applied to the bead is equal to zero; in what follows, the bead's position is calculated at each step so that the sum of all elastic forces from the motor links has to be equal to zero when no viscous load and thermal noise are present.

For each time step, we visit each of the N motors and determine their tentative states (attached or detached) and positions. During the updating procedure, at each computational step, each motor's state is updated once. If the motor is currently

unattached, we allow it to attach with a probability $P_{on} = \pi * \Delta t$, determined by the on rate π, to any binding site on the track within distance l on either side from the bead's center of mass. If the motor is currently attached, a load F_i felt by the ith motor is obtained by multiplying the extension of its link Δl_i by the link's stiffness k, and there are three possibilities: The motor can remain stationary, advance, or detach. Probabilities of these three events are determined from the single-motor model based on the current load on the motor: (*i*) P_{off} is calculated using Eq. **S3** irrespective of the direction of the force applied to the motor; (*ii*) P_{step} is calculated using Eq. **S2** for backward loads $F_i < F_s$; for backward load greater than F_s, $P_{step} = 0$; a forward load does not alter the motor cycle, so we substitute $F_i = 0$ for forward loads in Eq. **S2**. If the motor steps, its position x_i is changed to $x_i + d$. When we determine the tentative states and positions of all N motors, we update the states and positions of all motors simultaneously. Then, the number of engaged motors n and their locations are recorded and the bead position is updated.

Updating cargo position in the presence of viscous load and thermal noise. In the presence of the viscous load, the position of the bead is determined not by the balancing of the elastic motor forces to zero, but by the viscous force and thermal force that the bead experiences. In the absence of any force, the bead would execute a Brownian motion due to the thermal noise. Over a time interval of Δt, the displacement of the bead due to these thermal kicks can be drawn from a normal distribution with a mean-square displacement $2D\Delta t$, where D is the diffusion constant of the bead. We neglected the thermal motion of the linkages. If the bead is subjected to the net force f, this causes it to move with velocity $v_{drift} = f/\gamma$. The net motion of the bead over the time interval Δt is given by the sum of deterministic drift $x_{drift} = v_{drift} * \Delta t$ and diffusion $2D\Delta t$ due to thermal noise. The net force f on the cargo is given by $f = \sum_i^N f_i$, where f_i is the elastic restoring force exerted by the ith linkage on the cargo, which magnitude depends on the extension of the ith linkage.

Stochastic model of bidirectional transport. The stochastic model of the unidirectional transport can be easily extended for the bidirectional transport by just adding motors that move in the opposite direction (which have different single-motor parameters, such as on rate, off rate, velocity, etc.). The length of the linkage for kinesin motors was taken as 110 nm, and the length of the linkage for dynein motors was taken as 50 nm. Calculation of the cargo position is done similar to the unidirectional case. In the absence of viscous drag and thermal noise, position of the cargo is calculated using the simple force balance. In the presence of thermal noise and viscous drag, the cargo position is calculated in the manner similar to the unidirectional case. However, in this case net force f is the sum of the forces exerted by both sets of motors moving in opposite directions.

Parameter Values Used. Fig. 3: (*A*) Parameter values used for the simulations of stochastic model were $v = 1$ μm/s, $k = 0.32$ pN/nm, $F_d = 4$ pN, $F_s = 5$ pN, $\pi = 5$/s, $\varepsilon = 1$/s with $\Omega(F) = \text{Exp}(F/F_d)$ for $F < F_s$ and $\Omega(F) = 1.07 + 0.186 * F$ for $F \geq F_s$. Simulations were started with the initial number of motors set to steady-state values. (*C*) Parameters used for mean-field models (MF, EXPT & MF, EXPN) were $N = 2$, $F_d = 4$ pN, $F_s = 5$ pN, $\pi = 5$/s, $\varepsilon = 1$/s. $\Omega(F) = \text{Exp}(F/F_d)$ for all F was used for exponential detachment kinetics (*B*) Parameter values used for the simulations of stochastic model were $v = 0.8$ μm/s, $k = 0.32$ pN/nm, $F_d = 0.87$ pN, $F_s = 1.25$ pN, $\pi = 5$/s, $\varepsilon = 1$/s with $\Omega(F) = \text{Exp}(F/F_d)$ for $F < F_s$ and $\Omega(F) = 1/(0.254 * (1 - \text{Exp}(-F/1.96646)))$ for $F \geq F_s$. Simulations were started with the initial number of motors set to steady-state values.(*D*) Parameters used for mean-field models (MF, EXPT & MF, EXPN) were $N = 2$, $F_d = 0.87$ pN, $F_s = 1.25$ pN, $\pi = 5$/s, $\varepsilon = 1$/s. $\Omega(F) = \text{Exp}(F/F_d)$ for all F was used for exponential detachment kinetics.

Table 1: (ST, 5 K ~ 5 D, NoTuning) Data was obtained from 100 simulated tracks with maximum duration of 30 s for five kinesin versus five dynein motors on a cargo with all motors initially attached to the microtubule. The radius of cargo was taken as 0.25 μm. Parameter values for kinesin were $v = 1$ μm/s, $k = 0.32$ pN/nm, $F_d = 2.00$ pN, $F_s = 2.50$ pN, $\pi = 5$/s, $\varepsilon = 0.71$/s with $\Omega(F) = \text{Exp}(F/F_d)$ for $F < F_s$ and $\Omega(F) = 1.535 + 0.186 * F$ for $F \geq F_s$. Parameter values for dynein were $v = 0.8$ μm/s, $k = 0.32$ pN/nm, $F_d = 1.74$ pN, $F_s = 2.50$ pN, $\pi = 5$/s, $\varepsilon = 0.4$/s with $\Omega(F) = \text{Exp}(F/F_d)$ for $F < F_s$ and $\Omega(F) = 1/(0.254 * (1 - \text{Exp}(-F/1.96646)))$ for $F \geq F_s$.

(ST, 5 K ~ 5 D, EXPT, WT) Data was obtained from 100 simulated tracks with maximum duration of 30 s for five kinesin versus five dynein motors on a cargo with all motors initially attached to the microtubule. (ST, 2.5 K ~ 2.5 D, EXPT, Mut) Data was obtained from a mixture of, 50 simulated tracks for three kinesin versus three dynein motors and 50 simulated tracks for two kinesin versus two dynein motors, on a cargo with all motors initially attached to the microtubule where each track had a maximum duration of 30 s.

The radius of cargo was taken as 0.25 μm. Parameter values for kinesin were $v = 0.57$ μm/s, $k = 0.32$ pN/nm, $F_d = 2.00$ pN, $F_s = 2.50$ pN, $\pi = 0.95$/s, $\varepsilon = 0.35$/s with $\Omega(F) = \text{Exp}(F/F_d)$ for $F < F_s$ and $\Omega(F) = 1.535 + 0.186 * F$ for $F \geq F_s$. Parameter values for dynein were $v = 0.85$ μm/s, $k = 0.32$ pN/nm, $F_d = 1.74$ pN, $F_s = 2.50$ pN, $\pi = 1.19$/s, $\varepsilon = 0.37$/s with $\Omega(F) = \text{Exp}(F/F_d)$ for $F < F_s$ and $\Omega(F) = 1/(0.254 * (1 - \text{Exp}(-F/1.96646)))$ for $F \geq F_s$.

(ST, 2.5 K ~ 2.5 D, EXPT, WT) Data was obtained from a mixture of 50 simulated tracks for three kinesin versus three dynein motors and 50 simulated tracks for two kinesin versus two dynein motors, on a cargo with all motors initially attached to the microtubule where each track had a maximum duration of 30 s. (ST, 1.5 K ~ 1.5 D, EXPT, Mut) Data was obtained from a mixture of 50 simulated tracks for two kinesin versus two dynein motors and 50 simulated tracks for one kinesin versus one dynein motor, on a cargo with all motors initially attached to the microtubule where each track had a maximum duration of 30 s.

The radius of cargo was taken as 0.25 μm. Parameter values for kinesin were $v = 0.52$ μm/s, $k = 0.32$ pN/nm, $F_d = 2.00$ pN, $F_s = 2.50$ pN, $\pi = 1.10$/s, $\varepsilon = 0.35$/s with $\Omega(F) = \text{Exp}(F/F_d)$ for $F < F_s$ and $\Omega(F) = 1.535 + 0.186 * F$ for $F \geq F_s$. Parameter values for dynein were $v = 0.80$ μm/s, $k = 0.32$ pN/nm, $F_d = 1.74$ pN, $F_s = 2.50$ pN, $\pi = 1.29$/s, $\varepsilon = 0.37$/s with $\Omega(F) = \text{Exp}(F/F_d)$ for $F < F_s$ and $\Omega(F) = 1/(0.254 * (1 - \text{Exp}(-F/1.96646)))$ for $F \geq F_s$.

(ST, 5 K ~ 5 D, EXPN, WT) Data was obtained from 100 simulated tracks with maximum duration of 30 s for five kinesin versus five dynein motors on a cargo with all motors initially attached to the microtubule. (ST, 2.5 K ~ 2.5 D, EXPN, Mut) Data was obtained from a mixture of 50 simulated tracks for three kinesin versus three dynein motors and 50 simulated tracks for two kinesin versus two dynein motors, on a cargo with all motors initially attached to the microtubule where each track had a maximum duration of 30 s.

The radius of cargo was taken as 0.25 μm. Parameter values for kinesin were $v = 0.50$ μm/s, $k = 0.32$ pN/nm, $F_d = 0.60$ pN, $F_s = 2.50$ pN, $\pi = 0.9$/s, $\varepsilon = 0.26$/s with $\Omega(F) = \text{Exp}(F/F_d)$ for all F. Parameter values for dynein were $v = 0.75$ μm/s, $k = 0.32$ pN/nm, $F_d = 0.55$ pN, $F_s = 2.50$ pN, $\pi = 0.9$/s, $\varepsilon = 0.27$/s with $\Omega(F) = \text{Exp}(F/F_d)$ for all F

(ST, 3 K ~ 12 D, EXPT, WT) Data was obtained from 100 simulated tracks with maximum duration of 30 s for 3 kinesin versus 12 dynein motors on a cargo with all motors initially attached to the microtubule. (ST, 1.5 K ~ 6 D, EXPT, Mut) Data was obtained from a mixture of, 50 simulated tracks for two

kinesin versus eight dynein motors and 50 simulated tracks for one kinesin versus four dynein motor, on a cargo with all motors initially attached to the microtubule where each track had a maximum duration of 30 s. The radius of cargo was taken as 0.25 μm. Parameter values for kinesin were $v = 0.57$ μm/s, $k = 0.32$ pN/nm, $F_d = 4.00$ pN, $F_s = 5.00$ pN, $\pi = 1.25$/s, $\varepsilon = 0.35$/s with $\Omega(F) = \mathrm{Exp}(F/F_d)$ for $F < F_s$ and $\Omega(F) = 1.07 + 0.186 * F$ for $F \geq F_s$. Parameter values for dynein were $v = 0.78$ μm/s, $k = 0.32$ pN/nm, $F_d = 0.87$ pN, $F_s = 1.25$ pN, $\pi = 0.50$/s, $\varepsilon = 0.37$/s with $\Omega(F) = \mathrm{Exp}(F/F_d)$ for $F < F_s$ and $\Omega(F) = 1/(0.254 * (1 - \mathrm{Exp}(-F/1.96646)))$ for $F \geq F_s$.

(MF, 5 K ~ 5 D, EXPT, WT) Data was obtained from 1,000 simulated tracks with total 1,000 attachment and detachment events for $N_+ = N_- = 5$ motors on a cargo with all motors initially attached to the microtubule. (MF, 2.5 K ~ 2.5 D, EXPT, Mut) Data was obtained from 1,000 simulated tracks with total 1,000 attachment and detachment events. Tracks with $N_+ = N_- = 3$ and $N_+ = N_- = 2$ were chosen with equal probability. All motors were initially attached to the microtubule.

Parameter values for kinesin were $v_{F+} = 0.52$ μm/s, $v_{B+} = 0.001$ μm/s, $F_{d+} = 2.00$ pN, $F_{s+} = 2.50$ pN, $\pi_+ = 0.28$/s, $\varepsilon_+ = 0.5$/s with $\Omega(F) = \mathrm{Exp}(F/F_d)$ for $F < F_{s+}$ and $\Omega(F) = 1.535 + 0.186 * F$ for $F \geq F_{s+}$. Parameter values for dynein were $v_{F-} = 0.70$ μm/s, $v_{B-} = 0.001$ μm/s, $F_{d-} = 1.74$ pN, $F_{s-} = 2.50$ pN, $\pi_- = 0.18$/s, $\varepsilon_- = 0.5/s$ with $\Omega(F) = \mathrm{Exp}(F/F_d)$ for $F < F_s$ and $\Omega(F) = 1/(0.254 * (1 - \mathrm{Exp}(-F/1.96646)))$ for $F \geq F_s$.

(MF, 5 K ~ 5 D, EXPN, WT) Data was obtained from 1,000 simulated tracks with total 1,000 attachment and detachment events for $N_+ = N_- = 5$ motors on a cargo with all motors initially attached to the microtubule.(MF, 2.5 K ~ 2.5 D, EXPN, Mut) Data was obtained from 1,000 simulated tracks with total 1,000 attachment and detachment events. Tracks with $N_+ = N_- = 3$ and $N_+ = N_- = 2$ were chosen with equal probability. All motors were initially attached to the microtubule. Linear force-velocity curves were used for both kinesin and dynein motors. Parameter values for kinesin were $v_{F+} = 0.99$ μm/s, $v_{B+} = 0.072$ μm/s, $F_{d+} = 2.06$ pN, $F_{s+} = 2.50$ pN, $\pi_+ = 2.25$/s, $\varepsilon_+ = 0.90$/s with $\Omega(F) = \mathrm{Exp}(F/F_d)$ for all F. Parameter values for dynein were $v_{F-} = 1.45$ μm/s, $v_{B-} = 0.067$ μm/s, $F_{d-} = 1.91$ pN, $F_{s-} = 2.50$ pN, $\pi_- = 1.95$/s, $\varepsilon_- = 0.96$/s with $\Omega(F) = \mathrm{Exp}(F/F_d)$ for all F.

Fig. S1: In stochastic model, average temporal duration of run was calculated from 10,000 configurations where each configuration was started with the initial condition of all N motors attached to microtubule. The common parameter values used in stochastic and mean-field models were $v = 1$ μm/s, $F_d = 4$ pN, $F_s = 5$ pN, $\pi = 5$/s, $\varepsilon = 1$/s with $\Omega(F) = \mathrm{Exp}(F/F_d)$ for $F < F_s$ and $\Omega(F) = 2$ for $F \geq F_s$. Additional parameters for stochastic model were $\Delta t = 10^{-5}$ and $k = 0.32$ pN/nm. In stochastic and mean-field models with exponential detachment kinetics, $\Omega(F) = \mathrm{Exp}(F/F_d)$ was used for all F.

Fig. S4: (*A*, *A1*, *B*, and *B1*) Parameter values same as ST, 5 K ~ 5 D, EXPT, WT in Table 1. (*C*, *C1*, *D*, and *D1*) Parameter values same as ST, 2.5 K ~ 2.5 D, EXPT, Mut in Table 1. (*E*, *E1*, *F*, and *F1*) Parameter values same as ST, 2.5 K ~ 2.5 D, EXPT, WT in Table 1. (*G*, *G1*, *H*, and *H1*) Parameter values same as ST, 1.5 K ~ 1.5 D, EXPT, Mut.

Fig. S8: (ST, 5 K ~ 5 D, EXPT) Parameter values same as ST, 5 K ~ 5 D, EXPT, WT in Table 1. (ST, 2.5 K ~ 2.5 D, EXPT) Parameter values same as ST, 2.5 K ~ 2.5 D, EXPT, WT in Table 1. (ST, 5 K ~ 5 D, EXPN) Parameter values same as ST, 5 K ~ 5 D, EXPN, WT in Table 1. (ST, 3 K ~ 12 D, EXPT) Parameter values same as ST, 3 K ~ 12 D, EXPT, WT in Table 1. (MF, 5 K ~ 5 D, EXPT) Parameter values same as MF, 5 K ~ 5 D, EXPT, WT in Table 1. (MF, 5 K ~ 5 D, EXPN) Parameter values same as MF, 5 K ~ 5 D, EXPN, WT in Table 1.

Fig. S9: (*A* and *C*) Parameter values same as Fig. 3*C*. (*B* and *D*) Parameter values same as Fig. 3*D*.

1. Kunwar A, Vershinin M, Xu J, Gross SP (2008) Stepping, strain gating, and an unexpected force-velocity curve for multiple-motor-based transport. *Curr Biol* 18:1173–1183.
2. Klumpp S, Lipowsky R (2005) Cooperative cargo transport by several molecular motors. *Proc Natl Acad Sci USA* 102:17284–17289.
3. Courty S, Luccardini C, Bellaiche Y, Cappello G, Dahan M (2006) Tracking individual kinesin motors in living cells using single quantum-dot imaging. *Nano Lett* 6:1491–1495.
4. Muller MJ, Klumpp S, Lipowsky R (2008) Tug-of-war as a cooperative mechanism for bidirectional cargo transport by molecular motors. *Proc Natl Acad Sci USA* 105:4609–4614.
5. Soppina V, Rai AK, Ramaiya AJ, Barak P, Mallik R (2009) Tug-of-war between dissimilar teams of microtubule motors regulates transport and fission of endosomes. *Proc Natl Acad Sci USA* 106:19381–19386.
6. Gross SP, Welte MA, Block SM, Wieschaus EF (2002) Coordination of opposite-polarity microtubule motors. *J Cell Biol* 156:715–724.
7. Haghnia M, et al. (2007) Dynactin is required for coordinated bidirectional motility, but not for dynein membrane attachment. *Mol Biol Cell* 18:2081–2089.
8. McKenney RJ, Vershinin M, Kunwar A, Vallee RB, Gross SP (2010) LIS1 and NudE induce a persistent dynein force-producing state. *Cell* 141:304–314.
9. Wang X, Schwarz TL (2009) The mechanism of Ca^{2+}-dependent regulation of kinesin-mediated mitochondrial motility. *Cell* 136:163–174.
10. Shubeita GT, et al. (2008) Consequences of motor copy number on the intracellular transport of kinesin-1-driven lipid droplets. *Cell* 135:1098–1107.
11. Ally S, Larson AG, Barlan K, Rice SE, Gelfand VI (2009) Opposite-polarity motors activate one another to trigger cargo transport in live cells. *J Cell Biol* 187:1071–1082.
12. Vershinin M, Carter BC, Razafsky DS, King SJ, Gross SP (2007) Multiple-motor based transport and its regulation by Tau. *Proc Natl Acad Sci USA* 104:87–92.
13. Mallik R, Petrov D, Lex SA, King SJ, Gross SP (2005) Building complexity: An in vitro study of cytoplasmic dynein with in vivo implications. *Curr Biol* 15:2075–2085.
14. Saxton WM (1994) Isolation and analysis of microtubule motor proteins. *Methods Cell Biol* 44:279–288.
15. Petrov DY, et al. (2007) Studying molecular motor-based cargo transport: What is real and what is noise? *Biophys J* 92:2953–2963.
16. Mallik R, Carter BC, Lex SA, King SJ, Gross SP (2004) Cytoplasmic dynein functions as a gear in response to load. *Nature* 427:649–652.
17. Kunwar A, Mogilner A (2010) Robust transport by multiple motors with nonlinear force-velocity relations and stochastic load sharing. *Phys Biol* 7:16012.
18. Klumpp S, Lipowsky R (2005) Cooperative cargo transport by several molecular motors. *Proc Natl Acad Sci USA* 102:17284–17289.
19. Jeney S, Stelzer EH, Grubmuller H, Florin EL (2004) Mechanical properties of single motor molecules studied by three-dimensional thermal force probing in optical tweezers. *Chemphyschem* 5:1150–1158.
20. Singh MP, Mallik R, Gross SP, Yu CC (2005) Monte Carlo modeling of single-molecule cytoplasmic dynein. *Proc Natl Acad Sci USA* 102:12059–12064.

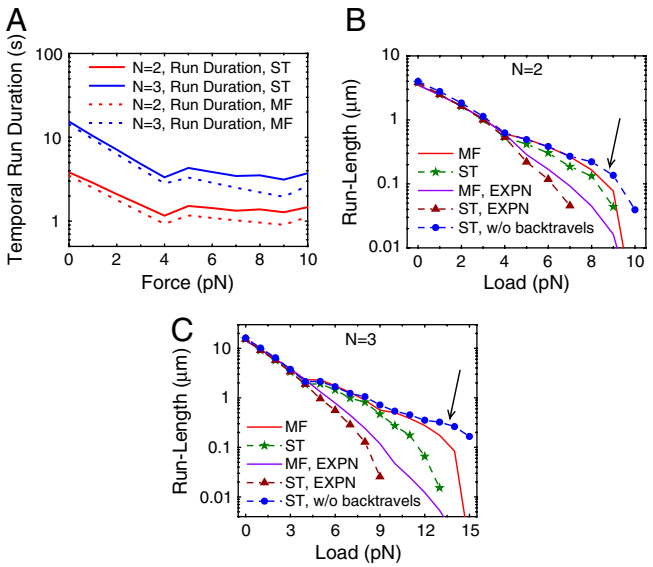

Fig. S1. (*A*) Force run duration and force travel distance relationships for different unidirectional models. For run durations, for otherwise identical parameter values (assuming exponential detachment-rate for $F < F_s$ and a constant detachment-rate, lower than detachment-rate at stall, for $F > F_s$), the stochastic model (ST) predicts slightly longer duration runs than the mean-field model, when there are two motors present ($N = 2$; red) or three motors present ($N = 3$; blue). When two or three motors are present (*B* or *C*, respectively), the predictions of the models depend on the assumptions. In particular, performance is lower with exponential detachment kinetics for both the stochastic (ST, EXPN) and mean-field (MF, EXPN) models, because of quick detachment under load, thus causing smaller run lengths. Performance is better for real detachment kinetics (MF or ST); however, it appears that for high load, the MF model has improved performance (red line above green line), in contradiction to the longer duration of the ST runs relative to the MF runs. This is explained by the back-travel present in the stochastic model (due to preferential detachment of the forward motor, and subsequent backward motion of the cargo's center of mass, discussed in Kunwar et al. (1), but absent in the MF model. Eliminating this backward motion from the ST model (for comparison), the ST model shows longer travel than the MF model (blue, marked with arrow).

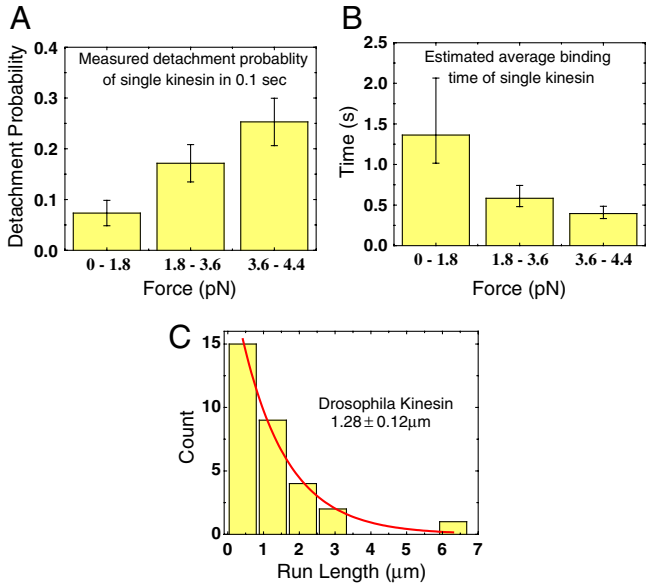

Fig. S2. Experimental characterization of single kinesin. The functional form used below stall of $\Omega(F) = \exp(F/F_d)$ implies that the off rate increases with load, which is somewhat different from the assumption in Kunwar et al. (1). To test the appropriateness of this assumption, we did the following. F_d was experimentally measured (see Fig. S6 below). Further, full-length kinesin was used in the optical bead assay to determine kinesin's approximate single-molecule detachment rate as a function of load, and indeed, whether or not it increased with load below stall. (*A*) The experimentally measured probability to detach in 0.1 s, for beads moved by single kinesins, characterized for low-load (0–1.8 pN) medium load (1.8–3.6 pN) and high load (within 0.1 pN of stall, including stall). Once this histogram was experimentally determined, the approximate probability of detachment per second was then estimated by multiplying the experimental probability by 10, and the corresponding expected duration of an event was then found by dividing this per second detachment probability into 1. The resultant expected durations are shown in the lower curve (*B*), and are consistent with the theoretical detachment-rate curve used in the simulations, shown in Fig. 2*G*. Kinesin purified from wild-type *Drosophila* embryos were used in the optical bead assay to study kinesin's single-molecule run length. (*C*) The experimentally measured distribution of run lengths for single kinesin. By fitting the distribution with decaying single exponential function (red curve) the average run length of single *Drosophila* kinesin is found to be 1.28 ± 0.12 μm.

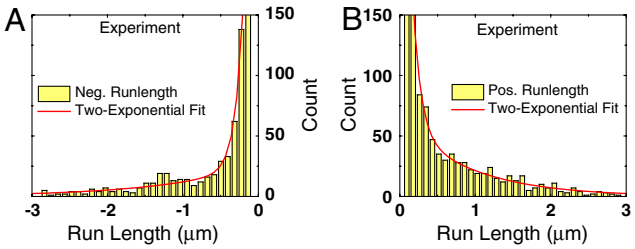

Fig. S3. Run-length distributions of lipid droplets in WT *Drosophila* embryo. Negative and positive run-length distributions of lipid droplets in WT embryos; the distributions were fit with the sum of two-decaying exponentials (red curve).

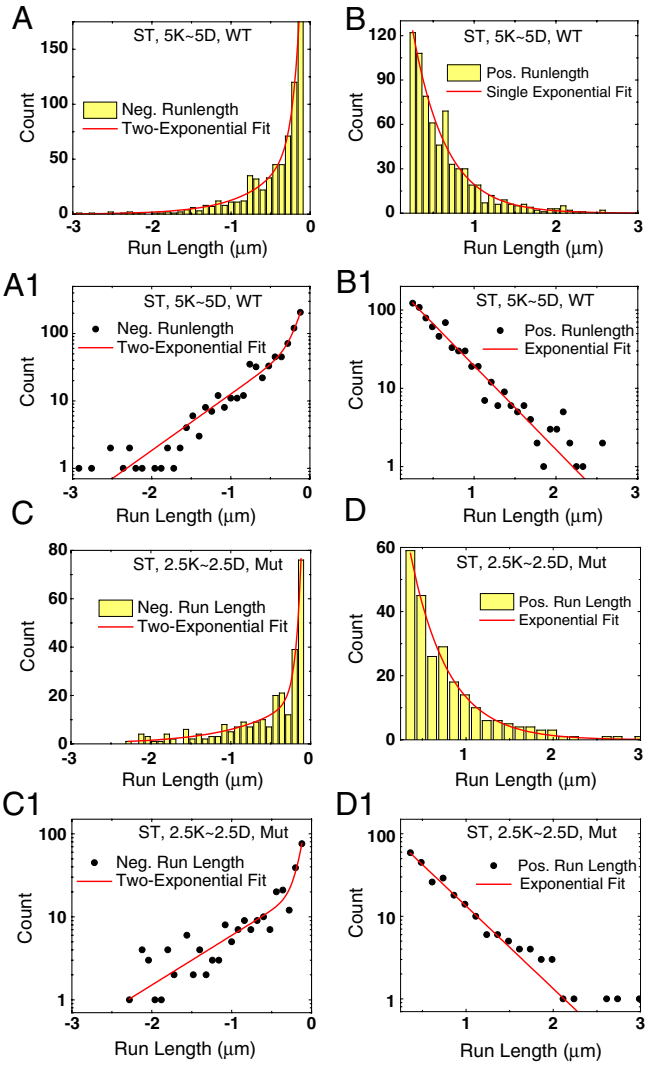

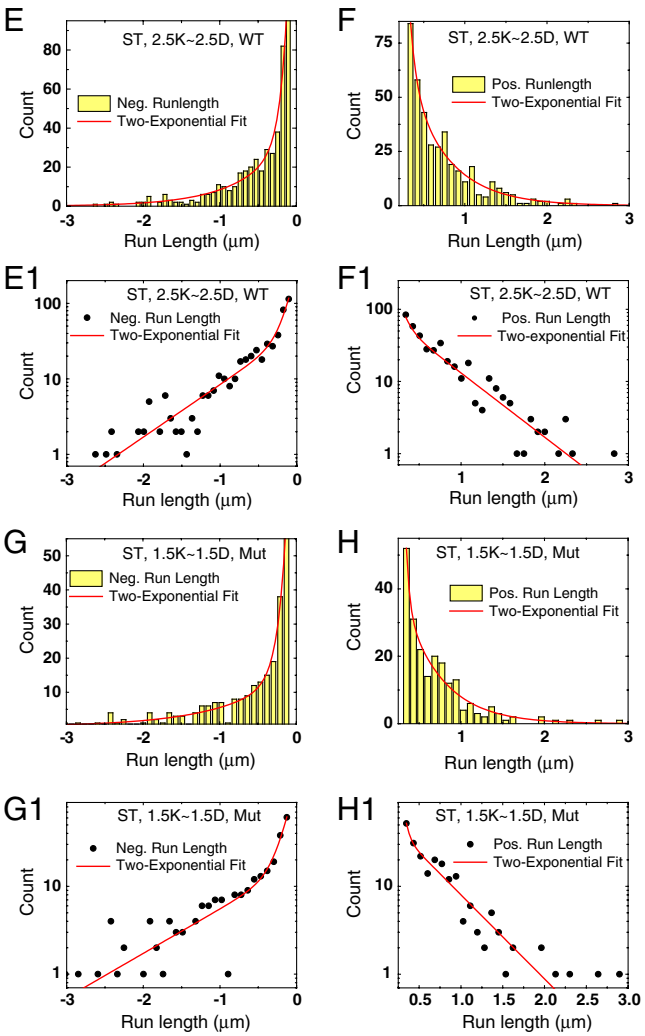

Fig. S4. Simulated run-length distributions for lipid droplets using ST models. The above plots illustrate simulated negative and positive run-length distributions obtained by using stochastic model (ST) with experimental detachment kinetics with $N = 5$ motors (*A*, *B*, *A1*, and *B1*), $N = 2.5$ motors (*E*, *F*, *E1*, and *F1*) and their corresponding mutants $N = 2.5$ motors (*C*, *D*, *C1*, and *D1*) and $N = 1.5$ motors (*G*, *H*, *G1*, and *H1*). Negative run-length distributions are fitted by sum of two-decaying exponentials as shown in the scattered plots with log scale. Distribution of positive run length for $N = 5$ motor case is single exponential, whereas for $N = 2.5$ motors the positive run length can be described by using two-exponential decays with a small dependence from shorter run length as illustrated in scattered plots *F1* and *H1*.

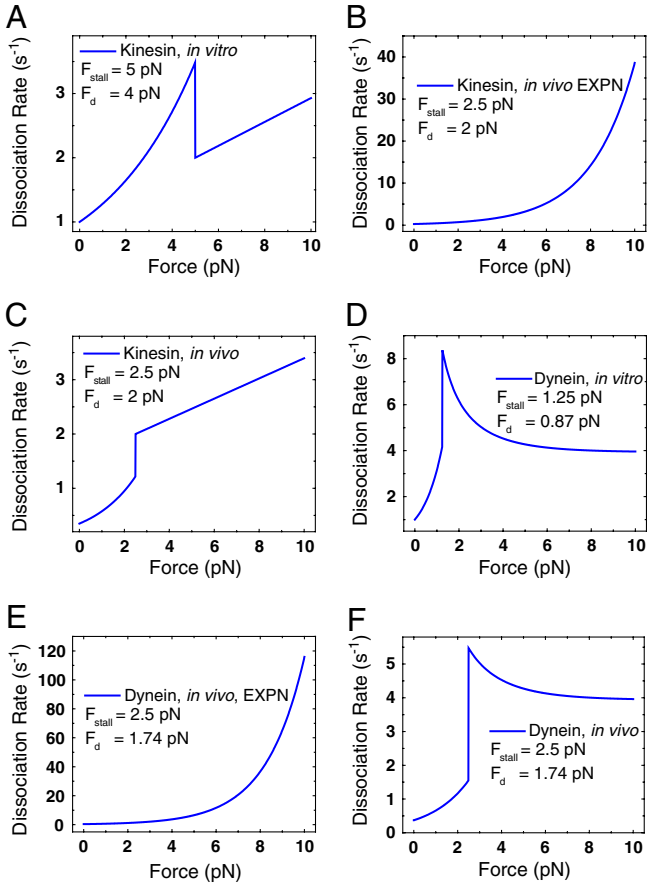

Fig. S5. Different force-dissociation kinetics used in this study. The in vitro experimentally constrained force-dissociation kinetics for kinesin is shown in *A*, and for dynein in *D*. These were modified to reflect the difference in stalling forces in vivo versus in vitro, to yield experimentally constrained in vivo force-dissociation kinetics for kinesin (*C*) and dynein (*F*). For kinesin, instead of $\Omega(F) = 1.07 + 0.186 * F$ appropriate for the in vitro case, we used $\Omega(F) = 1.535 + 0.186 * F$ so that that in vivo kinesin (*C*) has a dissociation rate of 2/s at stall. $\Omega(F)$ for dynein was unchanged. Past work assumed exponentially increasing detachment kinetics for kinesin (*B*) and dynein (*E*), and we considered these as well.

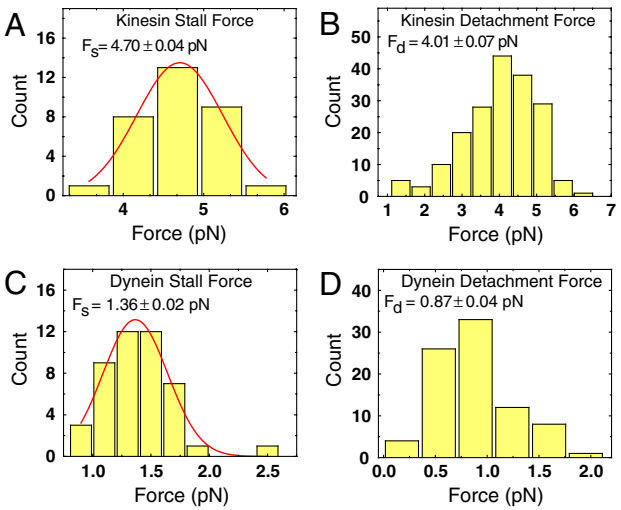

Fig. S6. Stall force and detachment force measurements. Experimentally determined stall force (F_s) and detachment force (F_d) distribution of single kinesin (*A* and *B*) and single dynein (*C* and *D*). Each stall-force distribution was fitted with a Gaussian function. The peak value of Gaussian function provides the mean of the stalling force. The distribution of detachment force is not symmetric and hence the mean value was obtained using the statistical average of the data.

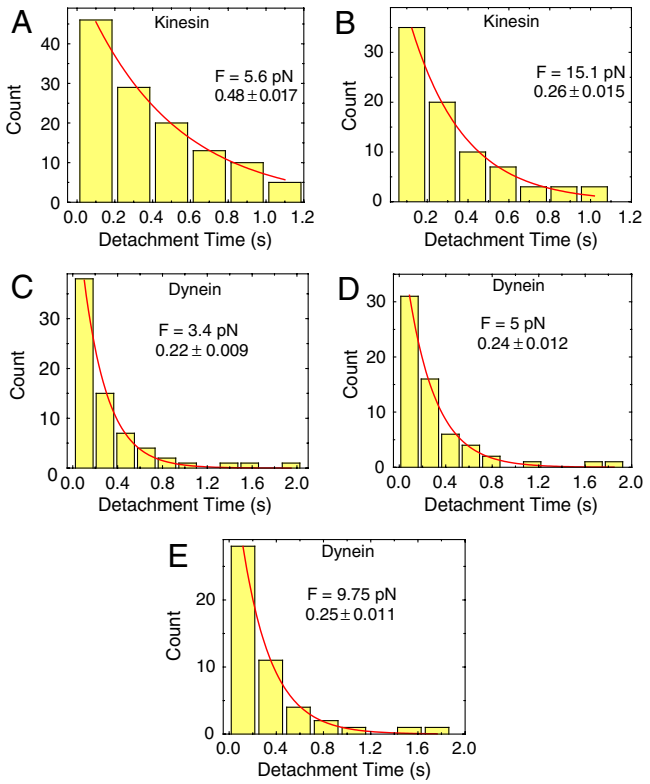

Fig. S7. In vitro single-molecule detachment kinetics at various loads: Histogram of experimentally measured detachment times for kinesin at force 5.6 pN (*A*) and 15 pN (*B*) and for dynein at 3.4 pN (*C*), 5 pN (*D*), and 9.75 pN (*E*) forces. The characteristic detachment times were determined by fitting the histograms with decaying exponentials.

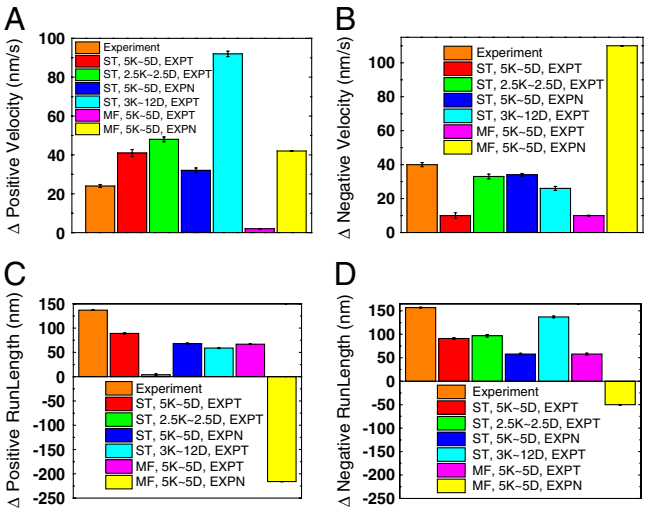

Fig. S8. Graphical representation of changes in velocity and run lengths between the wild-type and kinesin-dosage mutant, compared between experiment and the different theoretical predictions. In each case, from the mutant value we subtract the wild-type value, and the legend indicates the number of motors present in the wild-type version of the model; the mutant version has half as many. For instance, *D* shows that for the stochastic (ST) theory modeling the wild-type as having five motors (red) (and thus the mutant having 2.5 motors), the negative run lengths on average are predicted to be 80 nm longer in the mutant than in the wild-type. This compares with the experimental finding (orange) that in fact they are approximately twice this value.

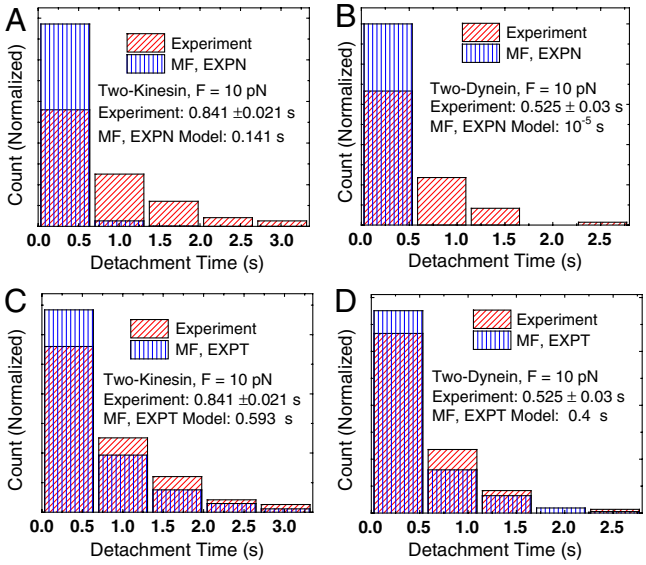

Fig. S9. Comparison of experimental measurements and unidirectional mean-field model predictions for detachment kinetics of two kinesin or dynein motors (histogram representation of additional data summarized in Fig. 3 *C* and *D*). The experimental conditions are described in Fig. 3 caption (main text). The distribution of detachment times (experimental bars, red hash marks; *A*, *B*, *C*, and *D*) was compared to the mean-field model with either experimental detachment kinetics (EXPT) or exponential detachment kinetics (EXPN). The single-molecule properties below stall (including single-motor detachment kinetics as measured in Fig. 2) constrained the model parameters as well. Using these constraints, the mean-field model with the EXPT detachment kinetics did not explain the experimental results (*C* and *D*), and the mean-field model with exponential detachment kinetics (EXPN) was even worse (*A* and *B*).